PREPARATION AND EVALUATION OF AOMKS FOR CATHEPSIN B IMAGING

PREPARATION AND EVALUATION OF PEPTIDYL ACYLOXYMETHYL KETONES FOR CATHEPSIN B IMAGING

By PATRICIA E. EDEM, B.Sc. (Hons.)

A Thesis Submitted to the School of Graduate Studies in Partial Fulfilment of the Requirements for the Degree of Master of Science

MASTER OF SCIENCE (2011) (Chemical Biology)

McMaster University Hamilton, Ontario

TITLE: Preparation and Evaluation of Peptidyl Acyloxymethyl Ketones for Cathepsin B

AUTHOR: Patricia Edim Edem, B.Sc. (Dalhousie University)

SUPERVISOR: Professor John Fitzmaurice Valliant

PAGES: xi, 62

Abstract

This thesis describes the initial steps towards the use of dipeptidyl acyloxymethyl ketones as a platform to develop molecular imaging (MI) probes for cancer. Initially the synthesis of an AOMK was performed following a literature procedure which resulted in an epimerized product. This issue was addressed by optimizing an alternative method yielding all intermediates in yields similar or better to those reported in the literature (final product yield of 67%). An AOMK derivative that can be used to evaluate target expression levels was synthesized by linking a fluorescent dye to the ε-amine group of lysine in accordance to a literature procedure describing the synthesis of an optical imaging probe in 24% yield. A second generation derivative AOMK was prepared by linking 4-fluoro-benzoic acid to the same amino group yielding a model of a PET MI probe.

An endpoint colorimetric assay was developed and optimized to test cathepsin B inhibitors. Due to the fact that the AOMKs exhibit time-dependent inhibition these assay conditions did not prove to be adequate for the assessment of the cathepsin B binding. Steps toward developing a continuous assay that would be better suited for these compounds were achieved. Factors such as the relationship between the formation of the assay product vs enzyme concentration and determination of the Michelis-Menten constant (K_m = 390 ± 30 nM) were established. These parameters can be used to determine the optimal enzyme and substrate concentration that should be used to test the AOMK based probes.

Acknowledgements

I would like to take this opportunity to thank the many people who have all helped to make this thesis possible. First and foremost I would like to thank my supervisor, Dr. John Valliant for his help, guidance, and encouragement throughout this work and the opportunity to work on an exciting and challenging project. I would also like to thank my committee members Drs Paul Harrison and Alex Adronov for useful suggestions and discussions and Dr. John Brennan as the director of the program. I'd also like to thank Kristina Trollip, Tammy Feher and the rest of the administrative staff in the department for their help throughout this process. I would also like to thank Dr. Laura Harrington for managing our research group as well as the Valliant group past and present.

I would also like to thank my wonderful family and friends for their love and support throughout this work. I would like to give a special thank you to my mother Dorothy Edem for her endless support throughout this process.

Table of Contents

List of Figures

List of Schemes

List of Tables

List of Abbreviations and Symbols

[I]	inhibitor concentration
[S]	substrate concentration
^{18}F	fluorine-18
^{1}H NMR	proton nuclear magnetic resonance
^{99m}Tc	metastable technetium-99
AA	amino acid
ACN	acetonitrile
Ala	alanine
AMC	7-amino-4-methylcoumarin
AOMK	acyloxymethyl ketone
Ar	aryl
B_{max}	receptor concentration
BMK	bromomethyl ketone
Boc	*tert*-butoxycarbonyl
Bt	benzotriazole
Bz	benzoyl
cm^{-1}	wavenumbers (IR)
Cy5	cyanine 5 monofunctional dye, Potassium Salt
DMF	N,N-dimethylformamide
DMK	diazomethyl ketone
DMSO	dimethyl sulfoxide
DOTA	1,4,7,10-tetraazacyclododecane-1,4,7,10-tetraacetic acid
ECM	extracellular matrix
EDC	1-ethyl-3-(3-dimethylaminopropyl) carbodiimide) hydrochloride
EDTA	ethylenediaminetetraactic acid

ESA	effective specific activity
ESI-MS	electrospray ionization mass spectrometry
FDG	2-fluoro-2-deoxy-D-glucose
HCl	hydrochloric acid
HMK	halomethyl ketone
HPLC	high pressure/performance liquid chromatography
hr	hours
IBCF	isobutylchloroformate
IC_{50}	concentration at resulting in 50% of maximal activity
IR	infrared
J	coupling constant (NMR)
K_d	dissociation constant
K_i	inhibitory binding constant
k_i	rate of inactivation
K_m	Michaelis-Menten constant
k_{obs}	rate of inhibiton
LC-MS	liquid chromatography mass spectrometry
Lys	lysine
m/z	mass to charge ratio
Me	methyl
MES	2-(*N*-morpholino)ethanesulfonic acid.
MI	molecular imaging
min.	minutes
MMP	matrix metalloprotease
MRI	magnetic resonance imaging
N	normal

NHS	N-hydroxysuccinimide
NIRF	near-infrared fluorescence
NMM	N-methyl morpholine
NMR	nuclear magnetic resonance
PET	positron emission tomography
Ph	phenyl
Phe	phenylalanine
pNA	p-nitroanilide
ppm	parts per million
qNIRF-ABP	quenched near-infrared fluorescent activity-based probe
R_f	retention factor (TLC)
RT	room temperature
SA	specific activity
$SOCl_2$	thionyl chloride
SPECT	single photon emission tomography
T:NT	target to non-target
TEA	triethylamine
TFA	trifluoroacetic acid
THF	tetrahydrofuran
TLC	thin layer chromatography
t_r	retention time (HPLC)
uPA	urokinase plasminogen-activator
V_{max}	maximum rate
Z/CBz	carbobenzyloxy
γ	gamma
ν_0	initial rate

1 Introduction

1.1 Molecular Imaging

Molecular imaging (MI) encompasses a variety of techniques that share the ability to non-invasively visualize biological or biochemical processes *in vivo*, often leading to the characterisation of a disease in a quantitative manner.[1] In cancer, for example, the changes in cell biology occur prior to the physical appearance of macroscopic primary tumours or metastases. By detecting changes in the tumour biology, it is not only possible to predict the aggressive nature of a disease but earlier detection of the disease can occur as well. MI, which hones in on biochemical differences between healthy and diseased cells, can be used not only for early detection, but to gauge the extent of a disease and monitor its progression on a patient specific basis.[2] Advantages of MI over other techniques that examine tumour biology are the ability to observe the system *in vivo* without perturbing the system and the elimination of sampling errors associated with cell assay methods.[2]

MI occurs by detecting signals originating from molecules that interact with a specific biological target.[3] These signaling molecules tend to be radioactive, fluorescent, or exhibit a paramagnetic effect, and are detected by the appropriate device.[4] This includes magnetic resonance imaging (MRI), magnetic resonance spectroscopy, optical imaging, ultrasound, and nuclear imaging.[4-5] The nuclear imaging techniques single photon computed tomography (SPECT) and positron emission tomography (PET) are

considered to be the most sensitive imaging method clinically largely due to their ability to measure probes in the nanomolar and even picomolar ranges.[2, 4-5]

1.2 Single Photon Emission Computed Tomography

SPECT is an imaging modality that detects signals from gamma ray emitting radionuclides. Isotopes such as gallium-67, iodine-123, indium-111, and technetium-99m are commonly used in nuclear medicine procedures.[6] When these SPECT isotopes decay, the gamma rays emitted are detected by a rotating gamma camera fitted with a collimator which acquires data at different angles during a 360° rotation around the patient. The 2-D projections acquired are then reconstructed to give a 3-D image.[7]

The metastable technetium-99 isotope (^{99m}Tc) is the most widely used radionuclide in nuclear medicine.[6b] Its 6.06 h half life and 141 keV γ-ray energy are ideal for imaging. The half-life is long enough to prepare the radiotracer, allow it to reach target tissue, and obtain useful diagnostic information, but short enough that the patient's radiation dose is minimized.[6b] The γ-ray emission energy is sufficient to penetrate tissues, and again low enough that the patient's radiation dose is minimized.[8] A further advantage is that ^{99m}Tc is conveniently obtained from a molybdenum generator. Here, ^{99}Mo in the form MoO_4^- is bound to an alumina (Al_2O_3) column and decays to $^{99m}TcO_4^-$, which is then eluted with a saline (0.9% NaCl) solution.[9]

The use of technetium as an imaging agent began in 1961 with pertechnetate ($^{99m}TcO_4^-$), used to image the thyroid gland.[8] A more recent example is ^{99m}Tc-sestamibi (Figure 1.1). This agent, typically used in myocardial perfusion imaging, also

accumulates in breast tumours. It accumulates in cells in accordance to perfusion, viability and mitochondrial activity.[10] When using this agent with a dedicated breast γ-camera it is possible to detect tumours in women with dense breasts that were not detected by traditional mammography.[11] This agent is however limited due to difficulties in detecting tumours less than 1 cm and there is a high rate of false positives where hematoma, inflammation, or fat necrosis occur.[12]

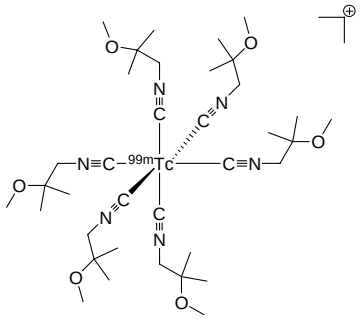

Figure 1.1 ^{99m}Tc-Sestamibi: used in SPECT imaging

1.3 Positron Emission Tomography

PET is an imaging modality that detects signals from positron emitting radionuclides.[13] Isotopes of carbon, nitrogen, oxygen and fluorine are typically used in clinical PET studies. When a PET isotope decays the positron emitted travels a short distance before colliding with an electron and undergoing an annihilation event. The collision results in the production of two gamma ray photons (511 keV), which travel approximately 180° from each other. The photons are detected simultaneously by a PET scanner comprised of a series of detectors arranged in a circular array around the

patient.[13] The simultaneous detection of the photons allows for the location of the probe in the body to be determined without the need of the collimator used in SPECT.

Fluorine-18 is the most widely used isotope in PET imaging. Similar to technetium-99m in SPECT imaging, the nuclear properties of ^{18}F make it attractive for PET imaging. Its 110 min half-life, although short, is longer than other typically used PET isotopes, yielding sufficient time for probe labelling and administration.[13] Some drawbacks of ^{18}F as an imaging agent is that there are not many naturally occurring fluorine containing biomolecules, so probe selection is limited. Even though ^{18}F can be used to replace a hydrogen atom, or a hydroxyl group in a molecule, the biological or physical properties of the fluorinated compound may significantly differ from the fluorine free analogue.[13]

An example of a PET agent used in imaging cancer is 2-fluoro-2-deoxy-D-glucose ([^{18}F]FDG, Figure 1.2). ^{18}FDG, which is structurally similar to glucose, shows uptake in most tumour cells, due to the increase in glycolysis in tumour tissue.[14] A major problem with using ^{18}FDG-PET in a whole body scan is that the sensitivity for breast cancer is quite low (64 – 90%) particularly for tumours less than 1 cm.[12b] Analogous to the dedicated breast γ-camera used in SPECT is positron emission mammography (PEM), which offers higher resolution and shorter imaging time than whole body PET scans and is therefore more effective than whole body PET for breast cancer imaging.[12b]

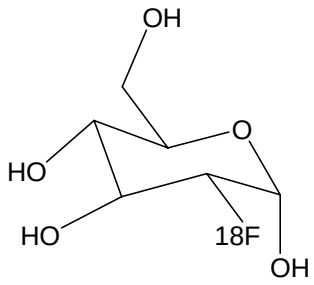

Figure 1.2 [^{18}F]FDG: PET imaging agent used in PEM

1.4 Probe Development

Radiopharmaceuticals generally fall into two broad categories: targeted probes and perfusion agents. Targeted probes demonstrate the occupancy of an enzyme or receptor site, while perfusion agents are distributed in accordance to a physical process such as blood flow, reflecting the functions of high capacity systems.[15] Targeted probes used in nuclear medicine tend to contain three main components: a *targeting vector* used to interact with the site of interest (enzyme, receptor, etc.), which is in turn attached to the *radionuclide* via a *linker* group (Figure 1.3).[1b]

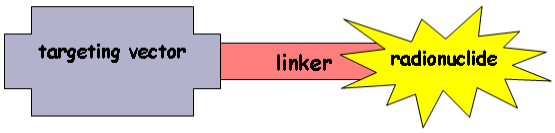

Figure 1.3 Schematic of a typical nuclear molecular imaging probe

When developing a molecular imaging probe there are a number of factors that need to be considered. Key considerations include: (a) choosing a target specific to the disease of interest that is overexpressed to an extent that it can be observed *in vivo* and that imaging this change provides useful information that impacts patient care; (b)

choosing a vector (antibody, peptide, enzyme, receptor ligand) that has high target affinity and that can access the tissue/region of interest; (c) determining stability, clearance route, kinetics, binding specificity, and target to non target (T:NT) ratio of the tracer *in vivo*; and (d) translation of the *in vivo* animal model systems to those applicable to humans in a clinical setting.[16]

When developing a probe to be used in nuclear imaging there are additional factors to consider regarding the isotope. Key ones include: (a) choosing an isotope that is readily available and affordable; (b) ensuring that its half-life compares well with the nature of the vector; and (c) ensuring that it is clinically useful and that it minimizes the radiation dose to the patient.[17]

It is also important when developing targeted nuclear MI probes to consider specific activity (SA) and effective specific activity (ESA). The SA is the amount of radioactivity of an element per mass of the total number of atoms of that element present in the sample while the ESA takes into account the total mass of everything that has affinity for the target. Any impurities that have affinity for the target would reduce the ESA even if the SA is unchanged which can impact the target to non-target ratios by competing with the agent for available target sites.[17-18]

PET and SPECT are two of the most clinically useful MI modalities available. Their use is restricted by the limited number of probes approved for routine clinical use. In order to use PET and SPECT as non-invasive imaging tools for diseases such as cancer, there is a need to develop new radiopharmaceuticals that fit the criteria described

above. In particular there is a need for agents that give information about the aggressiveness or metastatic potential of tumors.

1.5 Proteases and Cathepsin B

Proteases are enzymes which catalyze the hydrolysis of peptide bonds, in a process called proteolysis. This process is important in a number of normal physiological events but if left unregulated proteolysis can lead to a variety of disease states, such as cancer.[19] The hydrolysis of peptides is generally a slow process; therefore it requires the use of catalytic enzymes to drive the reactions. The five major classes of proteases (cysteine, serine, threonine, aspartic, and metallo-proteases) all share a common trait in that their active site involves a nucleophile and a general base.[19] In the case of cysteine proteases deprotonation of the thiol allows for nucleophilic attack on the electrophilic site of a substrate, followed by an attack by water at the carbonyl group (Figure 1.4).[20]

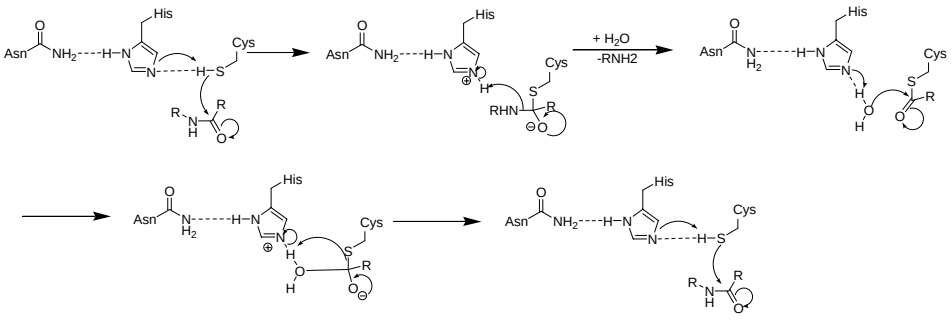

Figure 1.4 Proposed mechanism of action for cysteine proteases

The lysosomal protease, cathepsin B is the most studied of the cysteine proteases.[21] It is a glycoprotein with phosphate manosyl residues, as are all cathepsins and other lysosomal enzymes.[22] It can be found as 27 kDa or a 33 kDa protein in human fibroblasts

with the latter being the most active of the two.[22] The active site of cathepsin B contains cysteine (the nucleophile), histidine (the general base), and asparagine residues.[19, 23]

Cathepsin B is unique amongst other cysteine proteases in that it has the ability to act as an endopeptidase or exopeptidase due to the presence of an occluding loop.[24] The occluding loop is a segment of amino acids that block off one end of the binding cleft.[24-25] At low pH two salt bridges are formed and hold the loop in a closed position, this causes cathepsin B to act as an exopeptidase, removal of these salt bridges causes endopeptidase activity.[25]

1.6 Cathepsin B and Cancer

There are a number of characteristics of cancer, two major contributors to the overall aggressiveness of the disease are angiogenesis and metastasis.[20] For these processes to occur degradation of the extracellular matrix (ECM) is required.[20] There are a number of proteins present in the ECM, such as collagen, which are resistant to proteolysis from most proteases, and so protect the ECM from tumour invasion.[20] When cancer is present, tumours release a number of proteases capable of degrading the ECM.

Serine proteases, cysteine proteases, and matrix metalloproteases (MMPs) have been implicated in degrading the ECM in tumour metastasis.[20] It is possible that each protease plays a different role in certain types of cancers at specific times in tumour progression. The serine protease, urokinase plasminogen activating (uPA) enzyme and cathepsin B have shown a high level of activity at the invasive edge of a tumour.[20] Cathepsin B has a definite role in cancer metastasis, however, it is not clear if the protease

is directly responsible for the ECM degradation or if it activates other proteases involved in cancer progression (Figure 1.5).[20]

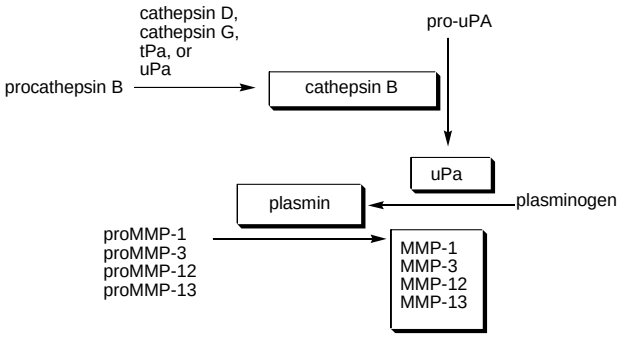

Figure 1.5 Activation cascade of proteases involved in metastasis

The primary cause of death in cancer patients is metastasis.[20, 26] The likelyhood that a tumour would spread is known as its metastatic potential and the amount of tumour spread (metastasis), or tumour staging, is a crucial prognostic factor for patients.[12b, 26] Cathepsin B has been implicated in its role in a variety of processes that are necessary for cancer progression. Although this enzyme is found in the lysosomes of normal cells it is also present in small amounts in the extracellular milleu, however it is highly overexpressed at the invasive edge of tumours.[20] Cathepsin B is therefore an attractive target for developing molecular imaging probes for assessing metastatic potential in cancers.

1.7 Targeting Cathepsin B

In order to target cathepsin B with an MI probe a vector capable of delivering the desired signaling molecule is required. One way to achieve this is by modifying a synthetic inhibitor of the protease. There are a variety of classes of inhibitors that

selectively target cathepsin B. These inhibitors can be grouped in terms of their mechanism of action. Various alkylating, acylating, phosphonylating, and sulfonylating agents have exhibited potent and selective inhibition of the protease.[19]

The majority of synthetic inhibitors of cathepsin B contain a peptide fragment for enzyme recognition and an electrophilic site for enzyme binding via the active site cysteine nucleophile.[20] A problem with inhibitors with highly electrophilic sites is their inherent chemical reactivity. This reduces the selectivity for the enzyme and its clinical usefulness due to the capability of reacting with other endogenous molecules.[19] The acyloxymethyl ketones are alkylating agents that represent a class of inhibitors that avoid this problem.

1.7.1 Acyloxymethyl Ketones

Acyloxymethyl ketones (AOMKs) in the form Z-[AA_1]-[AA_2]-CH_2OCOAr represent a class of compounds that have exhibited potent and selective inhibition of cathepsin B.[27] Prior to their discovery by Krantz *et al.*, halomethyl ketones (HMKs) were used as potent inactivators of the cysteine proteases, but their high chemical reactivity limited their clinical utility.[19, 27] The AOMKs have the ability to inhibit the enzyme, while the carboxylate leaving group reduces the overall chemical reactivity of the molecule.[19, 27] By varying the aryl carboxylate leaving group and the neighbouring amino acid (with Ala or Lys) a variety of AOMKs were tested *in vitro* and *in vivo* for cathepsin B inhibition. The compound that proved to be the most potent *in vivo* inhibitor was Z-Phe-Lys-$CH_2OCOPhMe_3$ (Figure 1.6) which exhibited a K_i of 170 nM *in vitro*.[27-28] The

AOMKs represent a class of potent cathepsin B inhibitors that although are subject to epimerization are otherwise chemically stable alternatives to HMKs.[28]

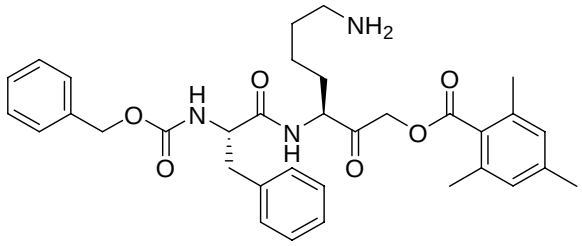

Figure 1.6 Z-Phe-Lys-$CH_2OCOPhMe_3$; a selective inhibitor of cathepsin B

1.7.2 Probes for Cathepsin B

An AOMK similar to that of Krantz *et al.*, (Z-Phe-Lys-$CH_2OCOPhMe_2$), has been used by Blum *et al.* in the development of quenched near-infrared fluorescent activity-based probes (qNIRF-ABPs). These compounds were used for whole body imaging in tumour bearing mice.[29] By modification at the epsilon nitrogen of lysine, fluorophores were incorporated into the molecule for optical imaging. The optical probe (GB123), containing a cyanine dye Cy5, as the fluorophore was injected into tumour bearing mice and the animals were imaged at various time points. Initially the fluorescence signal was present in nearly all tissues but as time progressed the NIRF signal concentrated in only the tumour tissues. In the case of the control (a probe lacking the electrophilic reactive site) the NIRF signal was not present in any tissues at the later time points (Figure 1.7).[29]

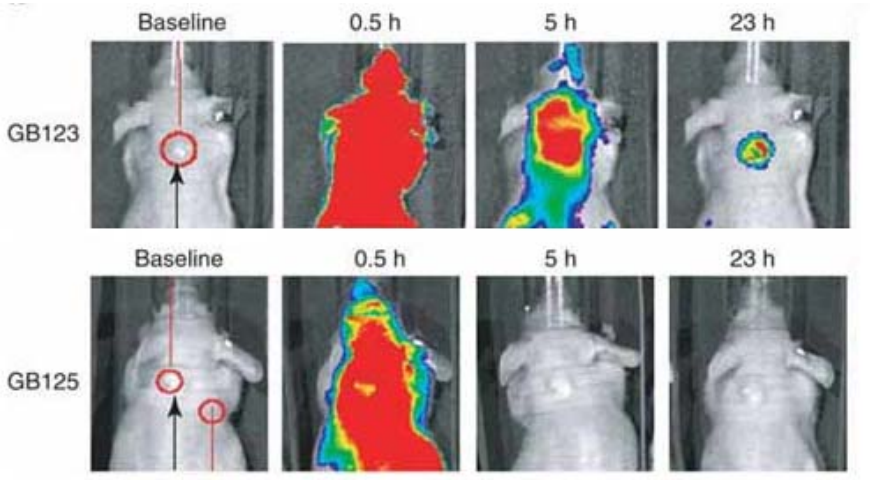

Figure 1.7 Optical images of living tumour bearing mice, with a fluorescently labelled AOMK cathepsin B probe (above) and a fluorescent labelled control that does not target cathepsin B (below).

This data suggests that an AOMK cathepsin B inhibitor can be modified such that it can act as an *in vivo* imaging probe. The major disadvantage of optical imaging is the inability to penetrate most tissues.[2] Optical imaging is limited to imaging subcutaneous lesions, but a radiolabelled probe with a radioisotope of suitable energy can address this issue and make an agent useful for clinical imaging. The authors also tested a ^{64}Cu labelled analogue that exhibited very low tumour uptake (0.14 – 0.3 % ID/g).[30] This poor uptake is likely due to changes in the pharmacokinetic properties of the probe, decreased cell permeability in comparison to the hydrophobic Cy5 containing probe and poor stability of the Cu-DOTA complex.[30-31]

1.8 Assessment of Cathepsin B Binding

Enzyme inhibition is an important strategy in the development of therapeutics and radiopharmaceuticals. The binding affinity of an inhibitor (K_i) is directly related to its

potency therefore determination of this parameter can give insights to how a probe might behave *in vivo*.[32] For a targeted MI probe, it has been established that at high specific activity the T:NT ratio is essentially equal to the ratio of the receptor concentration (B_{max}) and the dissociation constant (K_d, or K_i for an inhibitor).[33] It is therefore important to accurately determine parameters such as K_i for any probe that is to be tested *in vivo*.

Cathepsin B was the first lysomal protease to be homogenously purified and so is the most studied of the cysteine proteases.[22] One way to measure how cathepsin B activity is affected by inhibitors is by using substrates. In a substrate assay, the amount of cathepsin B activity is determined by measuring the amount of substrate that was hydrolysed by the enzyme. This is achieved by using a substrate that contains a leaving group that emits a measurable signal once it has been cleaved by the enzyme. Many studies have employed different fluorogenic substrates such as benzyloxycarbonyl-Arg-Arg-(7-amino-4-methylcoumarin, Figure 1.8 (Z-Arg-Arg-AMC) where the fluorescence from the leaving group following cleavage (ie. AMC) is measured.[27, 34]

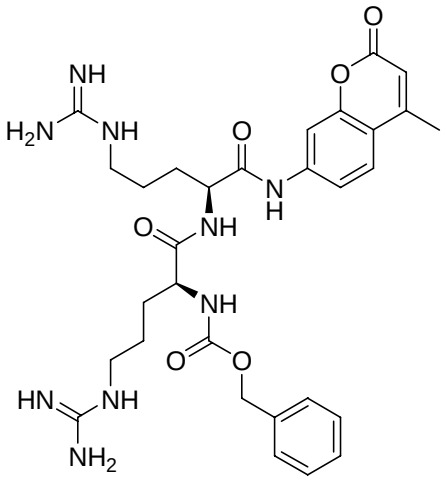

Figure 1.8 Z-Arg-Arg-AMC: a flurogenic substrate for cathepsin B

Alternately chromogenic substrates, like Z-Arg-Arg-pNA (benzyloxycarbonyl-Arg-Arg-(4-nitroanilide)) have been used as well where the absorbance of the yellow coloured pNA leaving group is measured.[34b, 34d, 35] Substrates of both types have been used in both stopped assays and continuous kinetic assays, with the fluorogenic substrates the most studied of the two classes especially in relation to irreversible inhibitors of cathepsin B and other papain-like proteases.

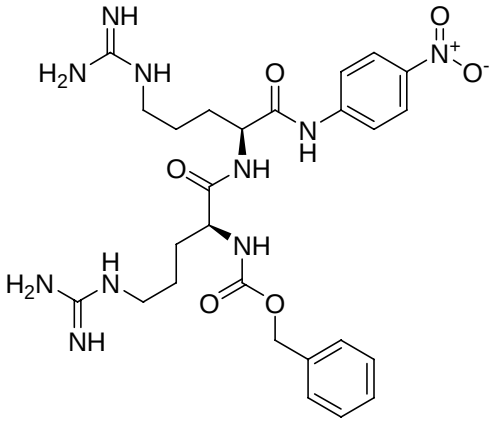

Figure 1.9 Z-Arg-Arg-pNA: a chromogenic substrate for cathepsin B

1.9 Rationale and Objectives

The objective of the current research is to create a platform for the development of cathepsin B molecular imaging probes and develop a robust assay to test them *in vitro*. Taking advantage of the fact that AOMKs are potent and selective inhibitors of cathepsin B, the approach taken was to first synthesize the phenylalanine, lysine derivative and incorporate signaling molecules at the *epsilon* nitrogen of its lysine side chain. The second goal was to develop a robust and facile colorimetric plate assay to assess the effect of incorporating these signaling groups on cathepsin B inhibition by the present and future AOMK derivatives.

2 Synthesis of Z-Phe-Lys AOMK and Derivatives: AOMK-II(Cy5) and AOMK(pFBz)

2.1 Synthesis of Z-Phe-Lys-$CH_2COPhMe_3$

The first step in the synthesis of the parent AOMK (**7**) was to prepare the N terminal protected phenylalanine-lysine dipeptide (**2**). It was prepared using either the methyl ester protected lysine (route A) or the benzotriazole activated phenylalanine (route B) as depicted in Scheme 2.1.

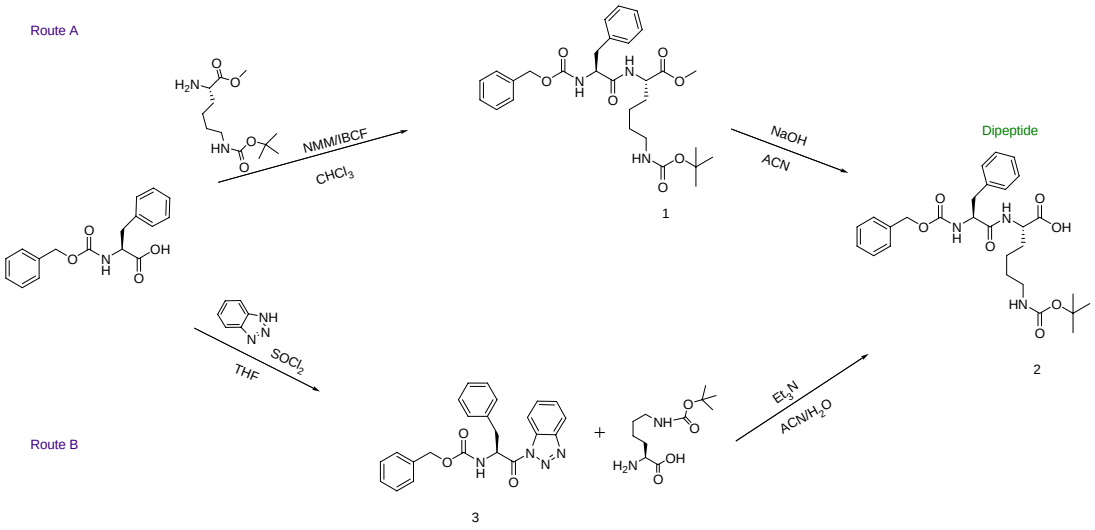

Scheme 2.1 Synthesis of Z-Phe-Ly(Boc)-OH dipeptide **2**

In route A, a procedure developed by Spezzacatena *et al.* to prepare dipeptides was employed here.[36] In this method the carbobenzyloxy (Cbz) protected phenylalanine was coupled to the side chain *tert*-butoxycarbonyl (Boc) protected methyl ester of lysine using isobutyl chloroformate (IBCF) in the presence of N-methyl morpholine (NMM) via

the mixed anhydride *in situ*. After successful coupling the dipeptide methyl ester (**1**) was isolated in 76% yield and then treated with sodium hydroxide to convert the dipeptide to the carboxylic acid. During work up any unreacted starting material was extracted with ethyl acetate. The aqueous layer containing the product was then neutralized with hydrochloric acid and then extracted with ethyl acetate. This hydrolysis reaction was originally performed in acetone as described in the literature[36] giving a yield of 67%. It was speculated that performing this reaction in acetone could lead to a competing reaction where the sodium hydroxide reacts with the ketone forming an enolate. This was potentially avoided by using acetonitrile (ACN) as the solvent instead and the yield was improved to 76%.

^{1}H NMR spectroscopy (Figure 2.1) of the isolated methyl ester showed singlets at 4.9, 3.6, and 1.3 ppm, which are diagnostic signals representing the methylene protons of the CBz protecting group, the methoxy protons, and the methyl protons of the Boc protecting group respectively. The diastereotopic methylene protons of the phenylalanine side chain appear as two separate signals at 3.2 and 2.7 ppm, while the majority of the protons in the lysine side chain show signals between 1.2 – 1.7 ppm. The protons adjacent to the amine of the Lys side chain show signals around 2.9 ppm. The alpha protons of lysine and phenylalanine appear at 4.2 and 4.3 ppm respectively.

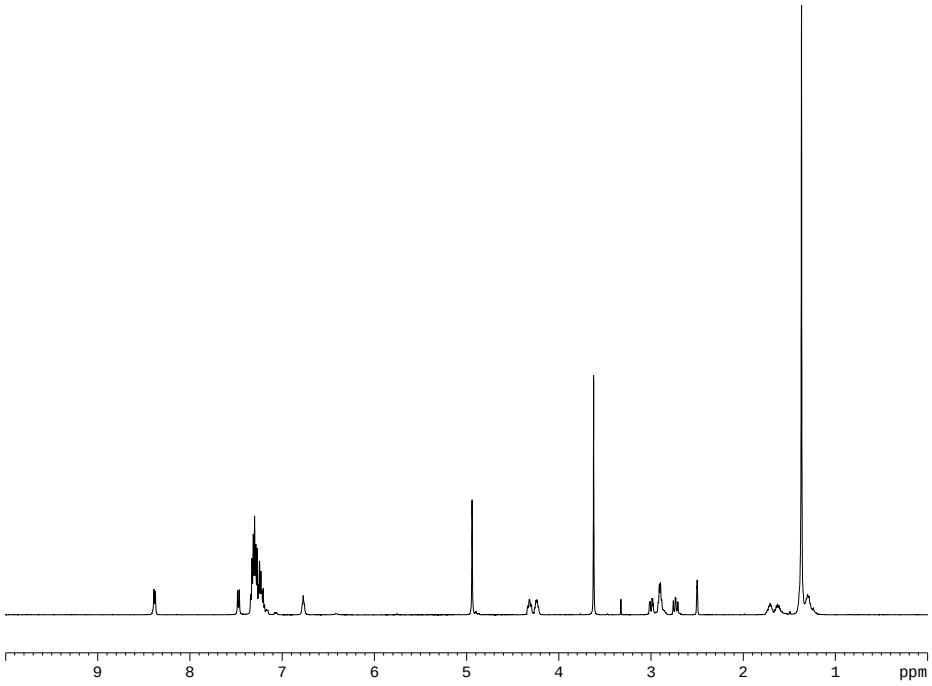

Figure 2.1 ^{1}H NMR (DMSO-d_6 , 500.13 MHz) of **1**

The ^{1}H spectrum of **2** was similar except that the singlet at 3.6 ppm representing the protons of the methyl ester was absent and a broad peak at 12.6 ppm representing the acidic hydroxyl group was apparent (Figure 2.2).

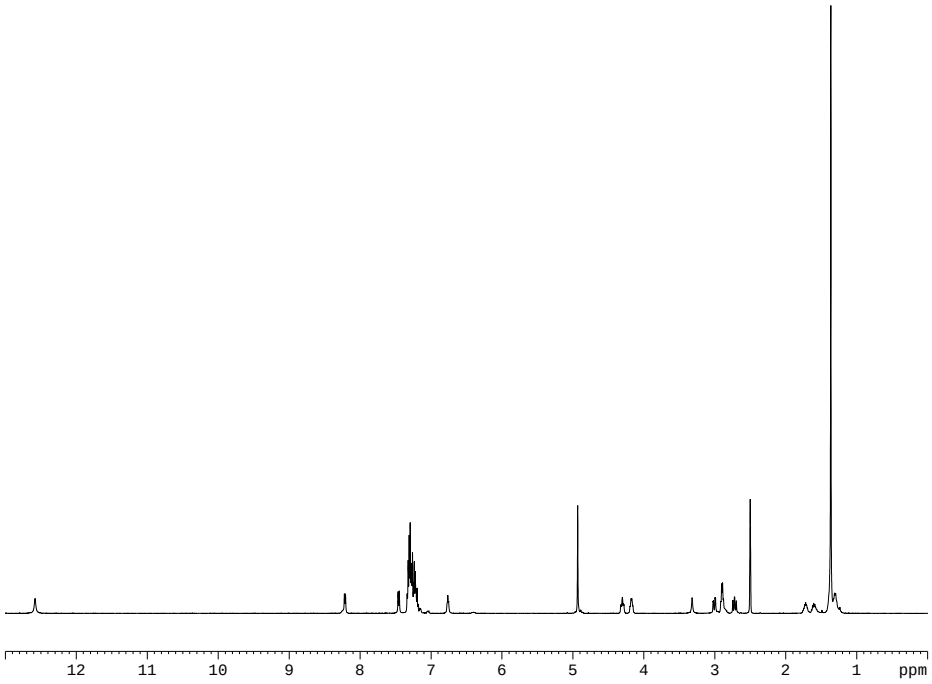

Figure 2.2 ^{1}H NMR (DMSO-d_6, 500.13 MHz) of **2**

Route B is an alternate procedure described by Katritzky *et al.* that was also used to prepare the dipeptides.[37] In this method Z-Phe-OH was converted to the activated benzotriazole (Bt) compound (**3**) using thionyl chloride ($SOCl_2$). During the reaction a white precipitate representing the hydrochloric acid (HCl) salt of the Bt formed and was removed by filtration. The remaining reaction mixture was washed with 6 N HCl to remove any unreacted Bt and the pure product was isolated in 74% yield.

^{1}H NMR spectroscopy (Figure 2.3) of **3** showed a singlet at 5.1 ppm representing the methylene protons of the CBz protecting group. The diastereotopic methylene protons of the phenylalanine side chain appear as two separate signals at 3.2 and 3.5 ppm. In the aromatic region the phenyl protons are apparent between 7.0 - 7.4 ppm and the

signals at 7.6, 7.7, 8.1 and 8.2 ppm represent the protons of the Bt group. The NH group can be seen at 5.6 ppm while alpha proton of phenylalanine appears at 6.0.

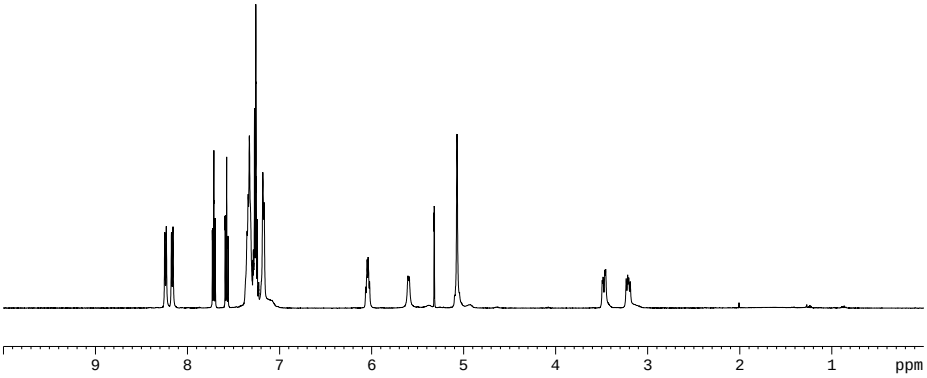

Figure 2.3 ^{1}H NMR ((CD_2Cl_2, 500.13 MHz) of **3**

The activated amino acid, Z-Phe-Bt (**3**) was then coupled to Nε-Boc protected lysine in the presence of triethylamine (TEA). During work up, the reaction mixture was washed with 6N HCl removing the Bt side product and the pure product was isolated in 82% yield.

The synthesis of **6** was originally reported by Krantz *et al.*[27] with a similar compound described by Blum *et al.* [38] The synthetic procedure used here was a scaled up procedure from the latter group. The first step was the conversion of the dipeptide to the diazomethyl ketone (DMK) via the mixed anhydride with IBCF in the presence of NMM and treating it with an excess amount of diazomethane in ether (Scheme 2.2).

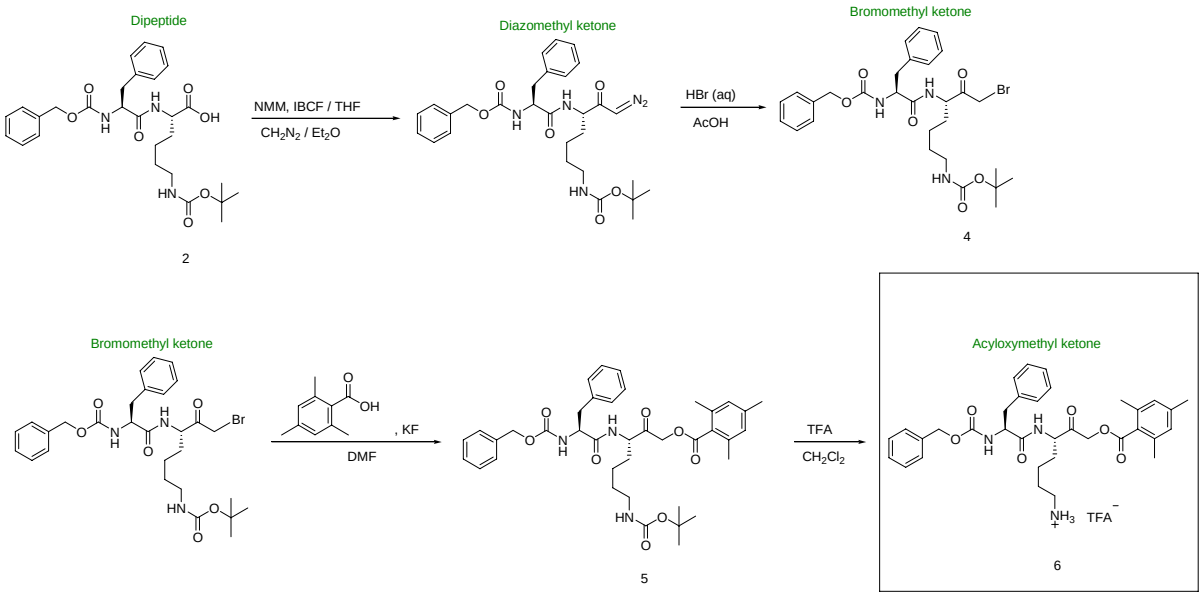

Scheme 2.2 Synthesis of Z-Phe-Lys-$CH_2COPhMe_3$ AOMK **6**

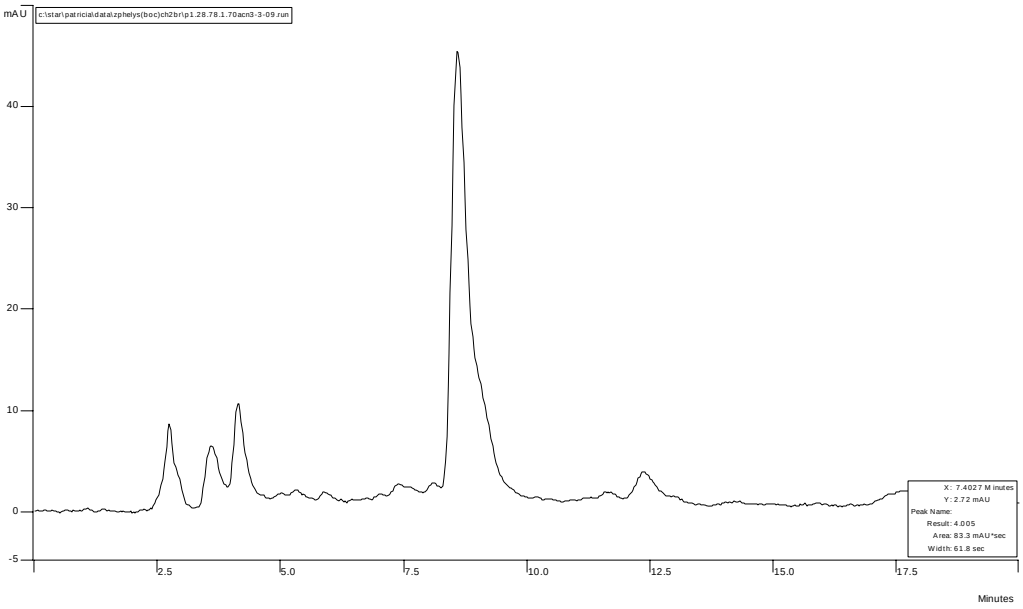

Figure 2.4 HPLC trace of Z-Phe-Lys-Br BMK **4** (T_R = 8.6 min)

Diazomethane was prepared from Diazald® using a specialized distillation kit as described by the supplier.[39] The resultant DMK, formed *in situ*, was then reacted with an

aqueous solution of hydrogen bromide in acetic acid generating the bromomethyl ketone (BMK) **4**. The acid solution was added at 0°C and only allowed to stir for 3 min. to prevent deprotection of the Boc group. **4** was isolated and used in the next step immediately without further purification. Prior to use, the purity of **4** was assessed using HPLC and the product eluted with 70% ACN, 30% H_2O at R_t = 8.6 min (Figure 2.4). The product was analyzed by ^{1}H-NMR as shown in Figure 2.5. The spectrum resembled that of **2** with the addition of 2 signals at 4.2 ppm associated with the additional diastereotopic methylene protons from the BMK **4**.

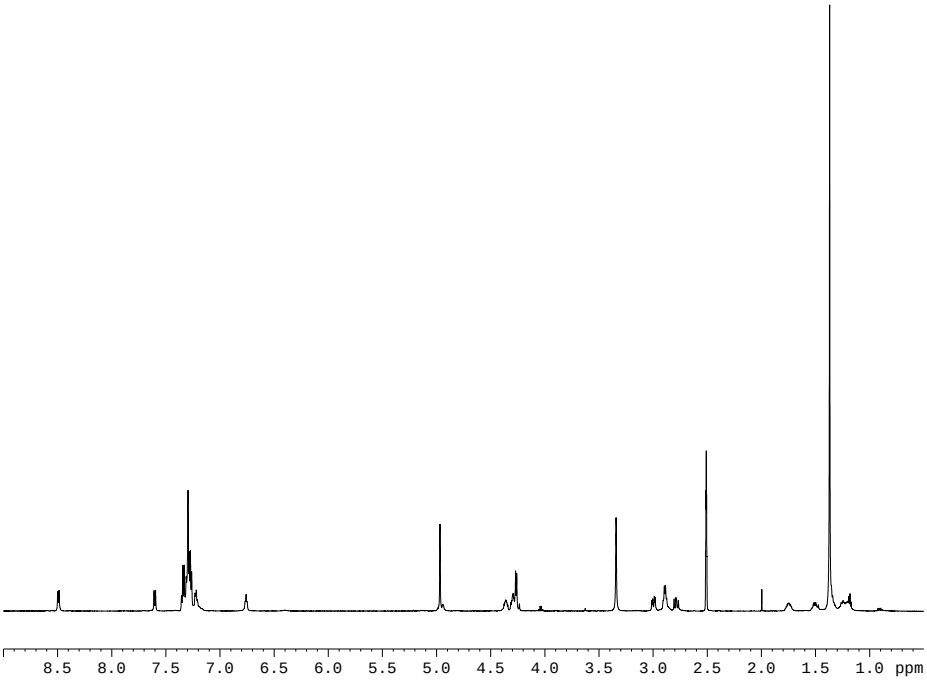

Figure 2.5 ^{1}H NMR (DMSO-d_6, 500.13 MHz) of **4**

The next step in the synthesis was the conversion of the BMK to the AOMK (**5**). **4** was mixed with 5 eq of the trimethyl benzoic acid and 10 eq of potassium fluoride (KF)

in DMF for 3 days. Reactions of this type can typically be performed in a few hours but due to the steric hinderance presented by the methyl groups on the acid a longer reaction time was needed. Following liquid-liquid extraction, the isolated product was analyzed by HPLC, however two compounds were eluted with 80% ACN at 10.8 and 11.3 min. Electrospray ionization mass spectrometry (ESI-MS) revealed the expected M+H (m/z = 688) and no mass representing the starting materials. This suggested, that the compounds present in the chromatogram are of the same mass, and are in fact isomers.

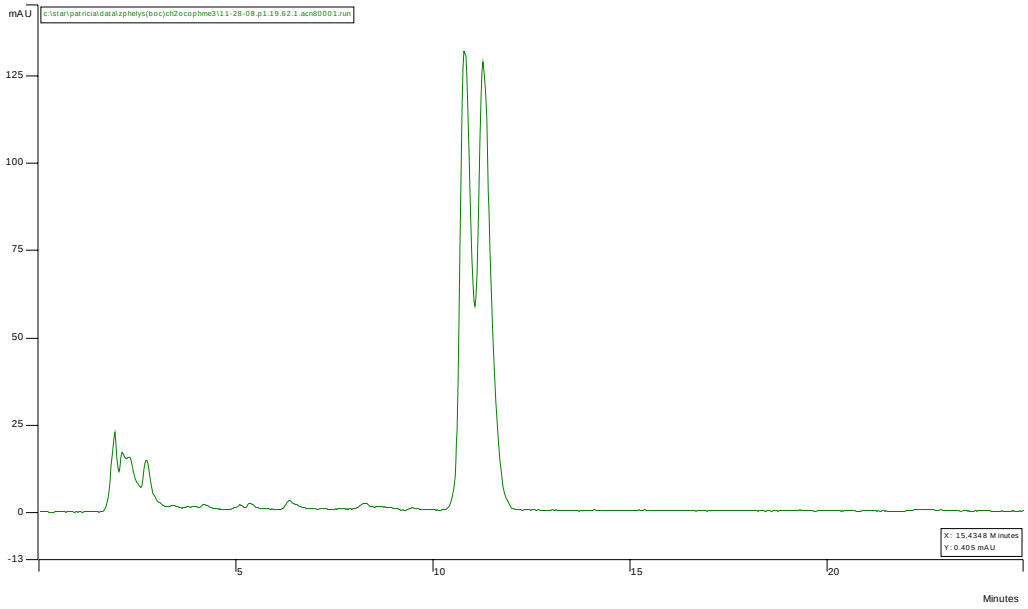

Figure 2.6 HPLC trace of isomers of Z-Phe-Lys(Boc)$CH_2COPhMe_3$ **5** (T_R = 10.8 and 11.3 min)

This deduction was further confirmed with ^1H NMR analysis (Figure 2.7). The spectrum showed a singlet at 6.9 ppm representative of the 2 additional aromatic protons in the trimethylbenzoate group, and two overlapping singlets at 2.2 and 2.3 ppm representing the 3 equivalent para methyl protons and the 6 equivalent ortho methyl

protons of the trimethylbenzoate group. The remainder of the spectrum was somewhat similar to the BMK but there were some additional signals in key areas. The amide protons (H_a) at 8.3 ppm appeared as two doublets, the methylene protons of the ketone (H_b) near 5.0 ppm showed additional splitting, as did the protons present in lysine (H_c) near 4.3 ppm. The integration of these signals in relation to the aromatic singlet indicated that these additional signals were signals from two different diastereomers.

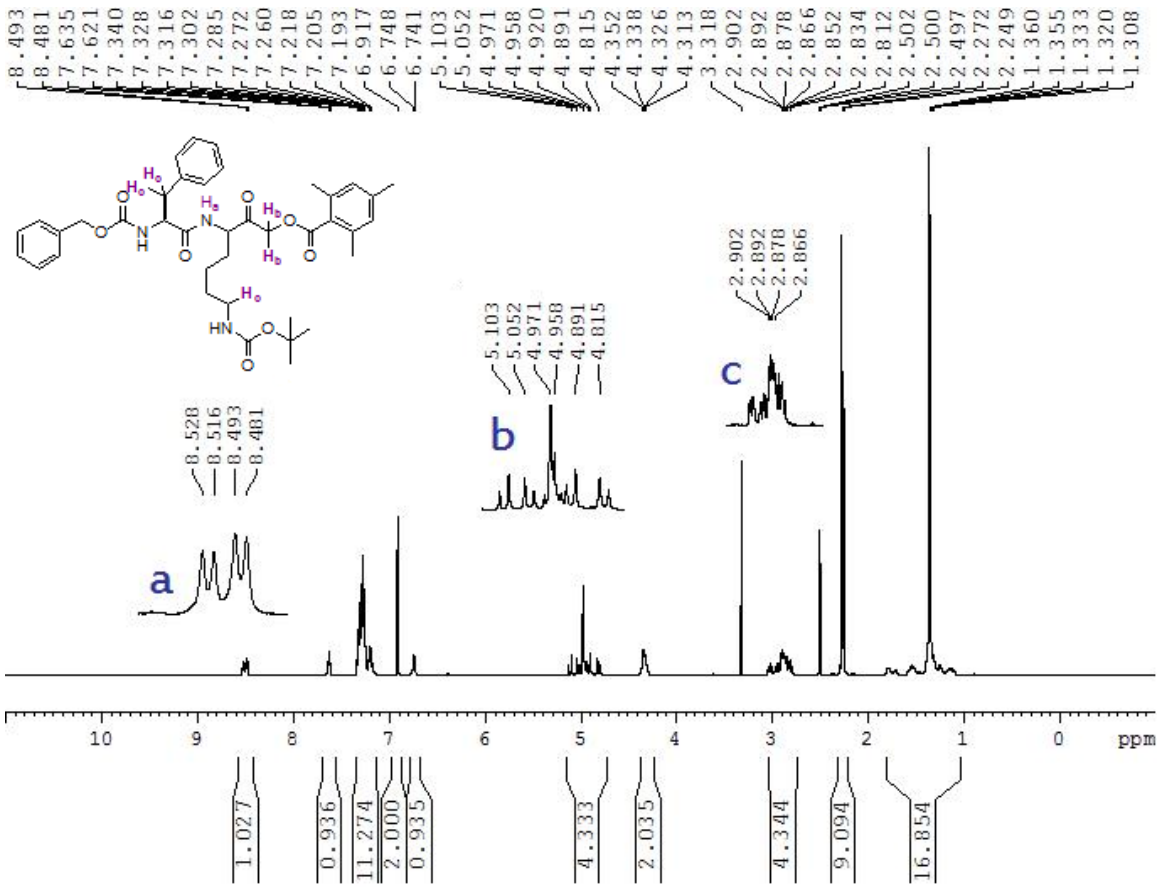

Figure 2.7 ^{1}H NMR (DMSO-d_6, 600.13 MHz) of **5** showing epimerization

The diastereomers likely arose as a result of epimerization of the lysine α proton that took place during the substitution reaction. It has been reported that synthesizing

AOMKs in the manner described here does not result in epimerization.[27] The long reaction time and large excess of potassium fluoride are the factors most likely to cause the epimerization. This issue was resolved by reducing the number of equivalents of the potassium fluoride and the benzoic acid derivative to perform the conversion of the **4** to **5**. By following a method used by Krantz *et al.*,[27] only 3 eq of KF and 1.1 eq of the benzoic acid were used and a single isomer was obtained. This was evident by the absence of the additional splitting in the ^{1}H-NMR (Figure 2.8).

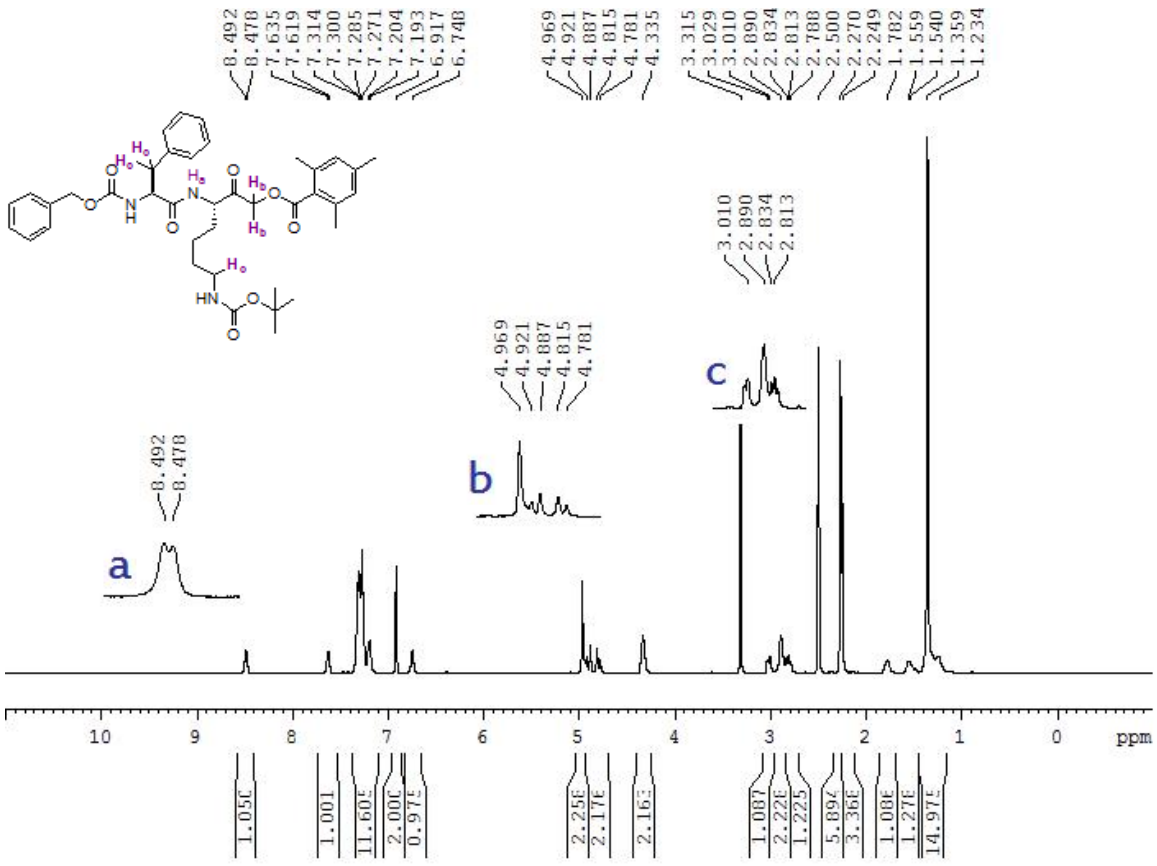

Figure 2.8 ^{1}H NMR (DMSO-d_6, 600.13 MHz) of **5** showing one isomer

The deprotection of the Boc group in **5** was conducted in dichloromethane with the dropwise addition of trifluoroacetic acid at 0°C, resulting in the TFA salt (**5**). The ^{1}H NMR of **6** was quite similar to that of **5** but the singlet at 1.3 ppm representing the tertbutyl methyl groups, is absent, confirming successful deprotection. ESI-MS was also in agreement showing a mass corresponding to the deprotected AOMK (m/z = 588).

2.2 Synthesis of Z-Phe-Lys(Cy5)-$CH_2COPhMe_2$

The optical images that resulted from the study by Blum *et al.*[29] showed very promising results as to the utility of the AOMK backbone for tumour targeting. The AOMK used to synthesize this probe differed in that the leaving group was a disubstitued benzoate group as opposed to the trisubstituted group. This AOMK was synthesized similarly to **5** and **6** where 2,6-dimethyl benzoic acid was used instead in order to mimic the optical probe (Scheme 2.3). The protected AOMK-II (**7**) was isolated in 74% yield and the deprotection occurred in 93% yield. The ^{1}H-NMR of **7** was similar to that of **5**. Notable differences were the absence of the singlet at 2.2 ppm from the methyl protons in the 4 position of the benzoate group and instead the presence of a signal at 7.1 ppm representing the proton in that position (Figure 2.9).

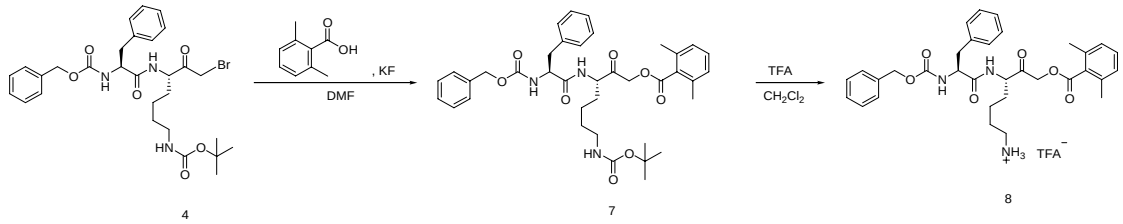

Scheme 2.3 Synthesis of *Z*-Phe-Lys-$CH_2COPhMe_2$ AOMK-II **8**

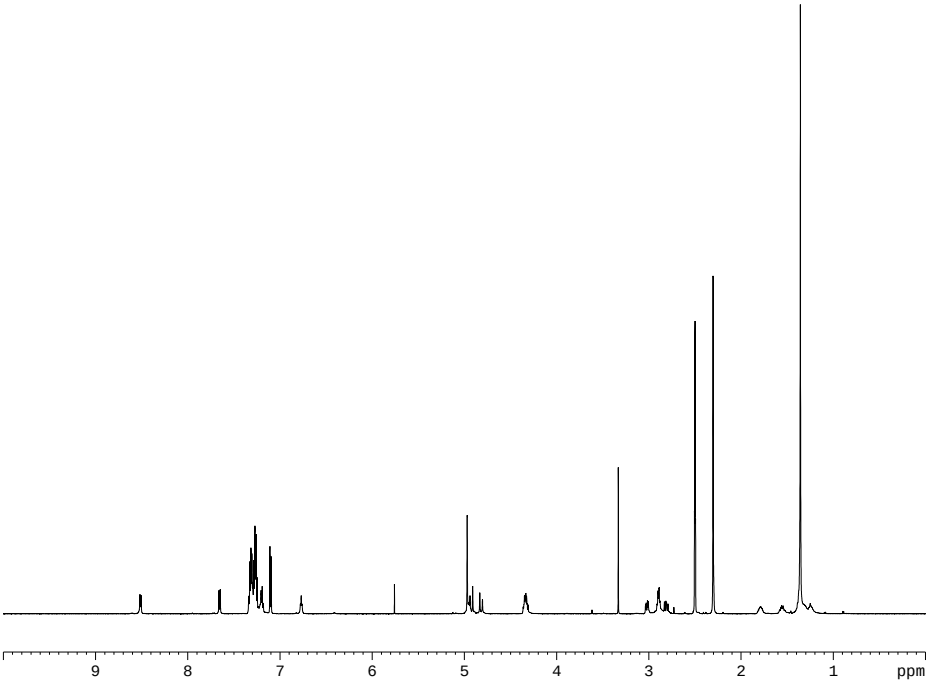

Figure 2.9 ^{1}H NMR (DMSO-d_6, 600.13 MHz) of **7**

The AOMK-II (**8**) was combined with the active ester of the cyanine dye giving the fluorescent probe (**9**) (Scheme 2.4). The reaction was performed in dimethyl sulfoxide (DMSO) for 3 hr at room temperature (RT) protected from light. The reaction mixture was purified by semi preparative HPLC and the desired product **9** was eluted with an ACN/water gradient (Figure 2.10). The product was isolated in 24% yield and the purity

and m/z of the product were confirmed using liquid chromatography-mass spectrometry (LC-MS) as described in the literature.[29]

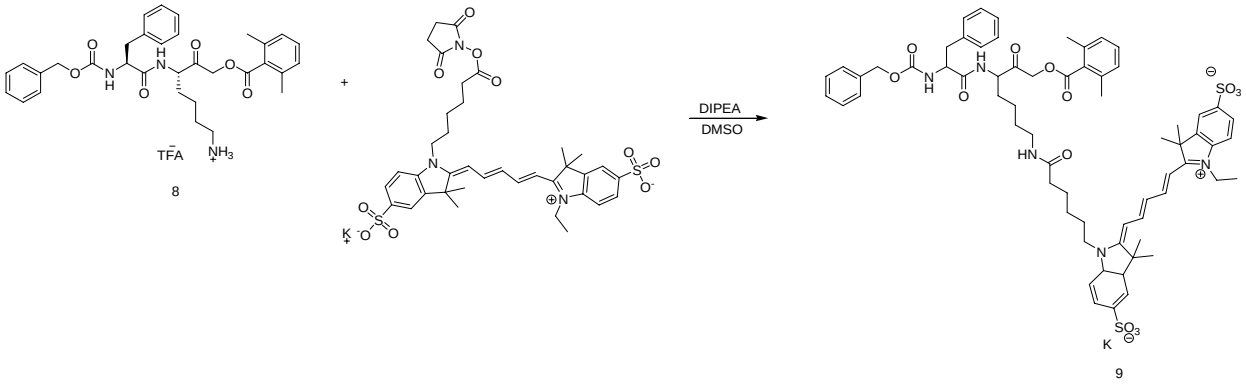

Scheme 2.4 Synthesis of Z-Phe-Lys(Cy5)-$CH_2COPhMe_2$ AOMK-II(Cy5) **9**

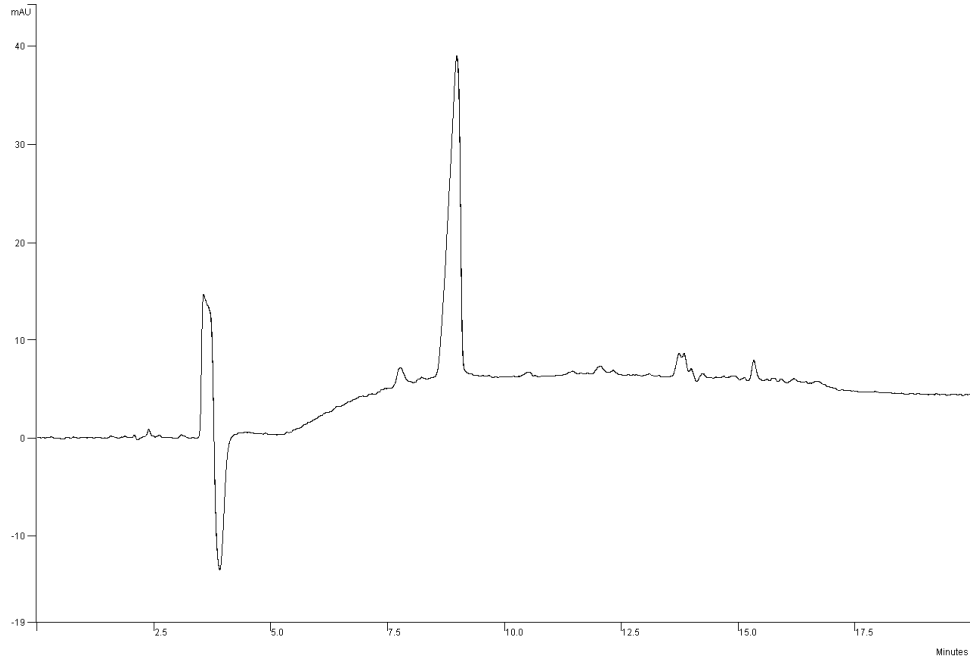

Figure 2.10 HPLC trace of Z-Phe-Lys(Cy5)-$CH_2COPhMe_2$ AOMK-II(Cy5) **9** (T_R = 8.9 min)

2.3 Synthesis of Z-Phe-Lys(pFBz)-$CH_2COPhMe_3$

The optical probe described previously showed promising results in tumour bearing mice however use of this probe is limited because it cannot be employed for whole body imaging. An analogous probe that could prove useful in humans is one in which a radioactive signaling molecule is used. Fluorine-18 is the most widely used isotope in PET imaging and it can be incorporated into the AOMK in a similar manner as the Cy5 dye. The initial aim was to prepare an AOMK linked to a ^{19}F prosthetic group as model compound for screening.

Following an established method used to radiolabel insulin with ^{18}F, 4-fluorobenzoic acid was converted to the activated N-hydroxysuccinimide (NHS) ester with 1-ethyl-3-(3-dimethylaminopropyl) carbodiimide (EDC) 92% yield[40]. The succinimidyl 4-fluorobenzoate (**10**) was then combined with the AOMK (**6**) in DMF in the presence of TEA and mixed for 3 hr (Scheme 2.5). Water was then added to the reaction and the crude product extracted with dichloromethane. The desired benzamide derivative (**11**) was isolated following column purification in 45% yield.

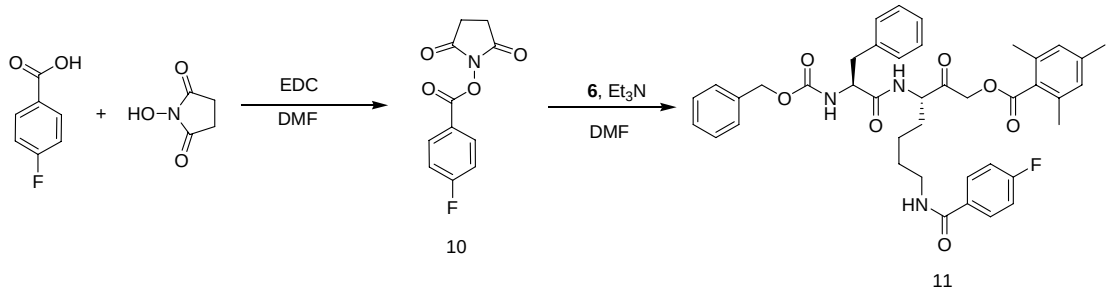

Scheme 2.5 Synthesis of Z-Phe-Lys(pFBz)-$CH_2COPhMe_3$ AOMK(pFBz) **11**

Compound purity was confirmed following analysis by ^{1}H NMR, analytical TLC and HPLC. The ^{1}H NMR spectrum of this compound was quite similar to that of (**6**) with the addition of signals in the aromatic region corresponding to the protons of the benzamide group at 7.9 and 7.3 ppm (Figure 2.11). ESI-MS was also in agreement showing a the expected mass (m/z = 710).

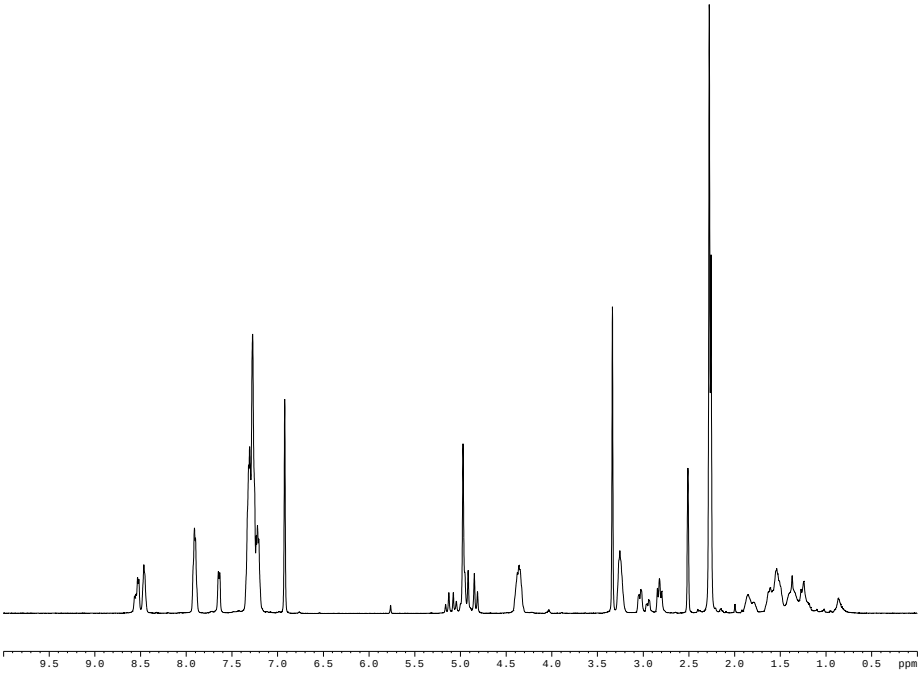

Figure 2.11 ^{1}H NMR (DMSO-d_6, 500.13 MHz) of **11**

2.4 Summary and Conclusions

The parent AOMK compound was synthesized by optimizing a literature method in such a way that epimerization did not occur and a single isomer was obtained. An additional AOMK was synthesized and derivatized with a fluroscent dye in accordance to

a literature procedure. To prepare the first potential fluorine-based PET analogue, a fluorobenzamide derivative of the initial AOMK was also prepared as a model of a PET MI probe. These compounds were prepared to utilize the AOMK backbone as a means to develop MI probes. The next phase was to screen compounds **9** and **11** against the parent AOMK derivative **6** using it as a positive control. If the ^{19}F derivative **9** has comparable affinity to **11**, future work would entail preparing and screening the radioactive analogue.

2.5 Experimental Section

2.5.1 Materials and Instrumentation

All chemicals were purchased from Sigma Aldrich, Novabiochem, or Bachem and used without further purification. Compounds **1** – **10** were prepared following literature procedures with slight modifications.[27, 36-37, 40] Diazomethane was prepared using the Diazald® Glassware Set with System 45® connections by Aldrich, as described in the literature.[39] The Cy5 succinimidyl ester was obtained from GE Healthcare. ^{1}H, ^{13}C, and 2D NMR spectra were recorded using either a Bruker AV500 or AV600 spectrometer. ^{1}H NMR signals are reported in ppm measured relative the residual proton signal of the deuterated solvent. Coupling constants (*J*) are reported in Hertz (Hz). ^{13}C signals are reported in ppm relative to the carbon signal of the solvent. Analytical TLC was performed on silica gel 60-F254 (Merck) plates and visualized using UV light. Infrared spectra were acquired using a BioRad FTS-40 FT-IR spectrometer. High resolution mass spectra were obtained on a Waters/micromass Q-ToF Ultima global spectrometer. Low resolution LC-MS was obtained on an Agilent 6340 Ion Trap LC/MS. HPLC was performed using a Varian Pro Star model 330 PDA detector, model 230 solvent delivery

system and a Phenomenex Gemini (L x ID = 100 x 4.6 mm) analytical column (5 μm C18). The semi-preparative column used was a Phenomenex Gemini (L x ID = 250 x 10 mm) analytical column (5 μm C18). The elution conditions were as follows: Method A:

Solvent A = acetonitrile, B = water: Elution Conditions: 30% A to 100% A 0 – 12 min; 100% A 12 – 24 min; 100% A to 90% A 20 – 28 min; 90% A to 30% A 28 – 30 min. The flow rate was set at 1 mL/min, monitoring at 254 nm.

2.5.2 Experimental Data

(S)-methyl-2-((S)-2-(Benzyloxycarbonyl)-3-phenylpropanamido)-6-(tert-butoxycarbonyl)hexanoate (1). Z-Phe-OH (1.49 g, 5 mmol) was dissolved in chloroform at -15°C and N-methylmorpholine (550μL, 5 mmol) was added. After 15 min. isobutylchloroformate (0.65 mL, 5 mmol) was added while maintaining the temperature at -15°C. After 10 min., H-Lys(Boc)-OMe·HCl (1.48g, 5 mmol) and N-methylmorpholine (550 μL, 5 mmol) were added and the reaction was mixed overnight. The solvent was removed by rotary evaporation and the resultant residue was dissolved in ethyl acetate (100 mL), washed with sodium bicarbonate (4 x 25 mL, 5% w/v), water (4 x 30 mL), 5% w/v citric acid (4 x 25 mL), and water (3 x 30 mL). The organic layer was dried over sodium sulfate and the solvent removed by rotary evaporation. The resultant oily residue was recrystallized from ethyl acetate/hexanes leaving a white powder. Yield (1.94 g, 76%). TLC (1:1 EtOAc:Hex): R_f =0.44; ^{1}H NMR (500.13 MHz, $(CD_3)_2SO$) δ 8.38 (d, J = 7.4 Hz, 1H N***H***CHCOOCH$_3$), 7.47 (d, J = 8.5 Hz, 1H N***H***CHCONH), 7.28 (m, 10H, ArH), 6.77 (m, 1H CH$_2$N***H***CO) 4.94 (s, 2H, PhC***H***$_2$O), 4.32 (m, 1H NC***H***CO in Phe), 4.24 (m, 1H NC***H***CO in Lys), 3.62 (s, 3H OC***H***$_3$), 2.99 (dd, J = - 13.9, 3.2 Hz 1H

CHC***H***$_2$Ph), 2.91 (dd, J = - 12.5, 6.3 Hz, 2H CONHC**H**$_2$), 2.73 (m, 1H, CHC***H***$_2$Ph), 1.71 (m, 1H, CHC***H***$_2$CH$_2$CH$_2$), 1.63 (m, 1H, CHC***H***$_2$CH$_2$CH$_2$), 1.36 (s, 9H, C(C**H**$_3$)$_3$), 1.36 & 1.30 (m, 4H C***H***$_2$C***H***$_2$CH$_2$NCO); ^{13}C NMR (150.91 MHz, (CD$_3$)$_2$SO) δ 172.5, 171.8, 155.8, 155.6, 138.0, 137.0, 129.2, 128.3, 128.0, 127.7, 127.4, 126.2, 77.3, 65.17, 55.80, 52.01, 51.79, 39.95, 37.39, 30.57, 29.06, 28.25, 22.65; HRMS Calcd. for $C_{29}H_{40}N_3O_7$ $[M+H]^+$: 542.2866. Found 542.2872; IR (KBr, cm^{-1}): 3317, 2951, 1740, 1690.

(S)-benzyl-1-(1H-benzo[d][1,2,3]triazol-1-yl)-1-oxo-3-phenylpropan-2-ylcarbamate (3). Excess amounts of 1H-benzotriazole (4.77 g, 40 mmol) were dissolved in 30 mL of anhydrous THF at 25°C under argon. Thionyl chloride (0.73 mL, 10 mmol) was added to the solution and stirred for approx 30 min. while warming to 35°C. Z-Phe-OH (2.99 g, 10 mmol) was dissolved in 10 mL of anhydrous THF and added to the reaction mixture dropwise at 0°C. The reaction was stirred for approx 3 hours. The white percipitate that formed during the reaction was filtered off. THF was removed by rotary evaporation leaving a white solid, which was dissolved in ethyl acetate (100 mL) and washed with 6 N HCl (3 x 50 mL) and brine (3 x 50 mL). The organic layer was dried over magnesium sulphate and the solvent removed by rotary evaporation to give a white powder which was recrystalized from chloroform/hexanes (1:1). Yield (2.95 g, 74%). TLC (1:2 EtOAc:Hex): R_f =0.53; ^{1}H NMR (600.13 MHz, (CD_2Cl_2) δ 8.24 (d, J = 8.2 Hz, 1H in Bt[ortho]), 8.17 (d, J = 8.2 Hz, 1H in Bt [ortho]), 7.71 (dd, J = 7.9, 7.7 Hz , 1H in Bt [meta/para]), 7.58 (dd, J = 8.0, 7.7 Hz , 1H in Bt [meta/para]), 7.07 – 7.35 (m, 10H in Ph), 6.02 - 6.06 (m, 1H NC**H**CO), 5.58 (d, J = 7.6 Hz, 1H CON**H**), 5.07 (s, 2H PhC**H**$_2$O), 3.47 (dd, J = 13.9, 4.7 Hz, 1H CHC**H**$_2$Ph), 3.21 (dd, J = 14.0, 8.1 Hz, 1H CHC**H**$_2$Ph); ^{13}C

NMR (150.90 MHz, (CD_2Cl_2) δ 171.5, 156.2, 146.7, 137.0, 135.9, 131.6, 131.4, 129.9, 129.2, 129.0, 128.7, 128.5, 127.9, 127.2, 120.9, 114.8, 67.6, 39.3; HRMS Calcd. for $C_{29}H_{40}N_3O_7$ $[M+H]^+$: 528.2710 Found 528.2704; IR (KBr, cm^{-1}): 3312, 2933, 1711, 1667.

(S)-2-((S)-2-(Benzyloxycarbonyl)-3-phenylpropanamido)-6-(tert-butoxycarbonyl)hexanoic acid (2). Route A. Z-Phe-Lys(Boc)-OMe **1** (2.00 g, 3.69 mmol) was dissolved in acetonitrile (10 mL) and 1 N NaOH (4 mL) was added. The solution was left to stir overnight at RT after which the solvent was removed by rotary evaporation and water (20 mL) was added. The solution was extracted with ethyl acetate (3 x 20 mL), and the aqueous layer neutralized with 1 N HCl (4 mL) at 0°C. The aqueous layer was extracted with ethyl acetate (3 x 20 mL) and dichloromethane (2 x 20 mL) and dried over magnesium sulfate. After filtration, the filtrate was concentrated to dryness. The oily residue was recrystalized from ethyl acetate/hexanes to give a white solid. Yield (1.48 g, 76%). TLC (2:1 EtOAc:Hex): R_f =0.41; ^{1}H NMR (500.13 MHz, $(CD_3)_2SO$) δ 12.76 (s, 1H, O***H***) 8.17 (d, J = 7.8 Hz, 1H N***H***CHCOOH), 7.47 (d, J = 9.0 Hz, 1H N***H***CHCONH), 7.26 (m, 10H, ArH), 6.76 (m, 1H CH_2N***H***CO) 4.94 (s, 2H, PhC***H***$_2$O), 4.30 (m, 1H NC***H***CO in Phe), 4.17 (m, 1H NC***H***CO in Lys), 3.02 (dd, J = -13.8, 3.0 Hz 1H CHC***H***$_2$Ph), 2.90 (dd, J = - 12.6, 6.6 Hz, 2H CONHC**H**$_2$), 2.73 (dd, -13.8 Hz, 10.8 Hz, 1H, CHC***H***$_2$Ph), 1.73 (m, 1H, CHC***H***$_2$$CH_2CH_2$), 1.61 (m, 1H, CHC***H***$_2$$CH_2CH_2$), 1.37 (s, 9H, C(C**H**$_3$)$_3$), 1.37 & 1.30 (m, 4H C***H***$_2$C***H***$_2$$CH_2$NCO); ^{13}C NMR (125.77 MHz, $(CD_3)_2SO$) δ 173.0, 171.5, 155.8, 155.6, 138.2, 137.0, 129.2, 128.3, 128.0, 127.7, 127.4, 126.2, 77.3, 65.2, 56.0, 52.1, 39.86, 37.4, 30.9, 29.2, 28.3, 22.7;

HRMS Calcd. for $C_{29}H_{40}N_3O_7$ $[M+H]^+$: 528.2710 Found 528.2704; IR (KBr, cm^{-1}): 3312, 2933, 1711, 1667.

Route B. H-Lys(Boc)-OH (0.91 g, 3.7 mmol) was dissolved in 5:2 acetonitrile/water (42 mL) in the presence of triethylamine (612 μL, 4.4 mmol) at RT. Z-Phe-Bt **3** (1.63 g, 4.07 mmol) was added and the reaction was left to stir overnight. The solvent was removed by rotary evaporation and water (25 mL) was added. 6N HCl (approx 5 mL) was added dropwise and the resultant percipitate was extracted with ethyl acetate (3 x 25 mL). The extracts were then washed with 6N HCl (3 x 20 mL), and brine (3 x 20 mL). The organic layer was dried over magnesium sulphate and the solvent removed by rotary evaporation. The oily residue was recrystalized from ethyl acetate/hexanes giving a white solid. Yield (1.60 g, 82%). TLC (2:1 EtOAc:Hex): R_f =0.41; ^{1}H NMR (500.13 MHz, $(CD_3)_2SO$) δ 12.76 (s, 1H, O***H***) 8.17 (d, J = 7.8 Hz, 1H N***H***CHCOOH), 7.47 (d, J = 9.0 Hz, 1H N***H***CHCONH), 7.26 (m, 10H, ArH), 6.76 (m, 1H CH_2N***H***CO) 4.94 (s, 2H, PhC***H***$_2$O), 4.30 (m, 1H NC***H***CO in Phe), 4.17 (m, 1H NC***H***CO in Lys), 3.02 (dd, J = -13.8, 3.0 Hz 1H CHC***H***$_2$Ph), 2.90 (dd, J = - 12.6, 6.6 Hz, 2H CONHC**H**$_2$), 2.73 (dd, -13.8 Hz, 10.8 Hz, 1H, CHC***H***$_2$Ph), 1.73 (m, 1H, CHC***H***$_2$$CH_2CH_2$), 1.61 (m, 1H, CHC***H***$_2$$CH_2CH_2$), 1.37 (s, 9H, C(C**H**$_3$)$_3$), 1.37 & 1.30 (m, 4H C***H***$_2$C***H***$_2$$CH_2$NCO); ^{13}C NMR (125.77 MHz, $(CD_3)_2SO$) δ 173.0, 171.5, 155.8, 155.6, 138.2, 137.0, 129.2, 128.3, 128.0, 127.7, 127.4, 126.2, 77.3, 65.2, 56.0, 52.1, 39.86, 37.4, 30.9, 29.2, 28.3, 22.7; HRMS Calcd. for $C_{29}H_{40}N_3O_7$ $[M+H]^+$: 528.2710 Found 528.2704; IR (KBr, cm^{-1}): 3312, 2933, 1711, 1667.

Z-Phe-Lys(Boc)-CH_2Br, BMK (4) Z-Phe-Lys(Boc)-OH **2** (2.00 g, 3.8 mmol) was

dissolved in anhydrous THF (20 mL) under argon at -10°C. *N*-methylmorpholine (522 µL, 4.75 mmol) and isobutylchloroformate (0.57 mL, 4.37 mmol) were added, and the reaction was allowed to stir for 25 min. at -10°C with the argon removed. An excess amount of diazomethane in ether was then added until the solution remained bright yellow at RT. The reaction was left to stir for 3 hrs, after which a solution of solution of 22% hydrogen bromide(22%) acetic acid (44%) and water (34%) (12.1 mL) was added dropwise at 0°C. After 3 min., the reaction was made up to 100 mL with ethyl acetate and the organic layer washed with water (3 x 30 mL), brine (3 x 30 mL), and saturated sodium bicarbonate (3 x 30 mL), and dried over magnesium sulfate. Removal of the solvent revealed a white powder that was used in the following step without any further purification. Yield (2.04 g, 89%). TLC (1:1 EtOAc:Hex): R_f =0.47; ^{1}H NMR (500.13 MHz, $(CD_3)_2SO$) δ 8.48 (d, J = 7.0 Hz, 1H N***H***CHCOCH$_2$), 7.59 (d, J = 8.2 Hz, 1H N***H***CHCONH), 7.27 (m, 10H, ArH), 6.75 (m, 1H CH$_2$N***H***CO) 4.96 (s, 2H, PhC***H***$_2$O), 4.35 (m, 1H NC***H***CO in Phe), 4.29 (m, 1H NC***H***CO in Lys), 4.26 (m, 2H, COC***H***$_2$Br), 2.99 (dd, J = - 13.6, 3.1 Hz, 1H, CHC***H***$_2$Ph), 2.88 (dd, J = - 12.6, 6.8 Hz, 2H CONHC**H**$_2$), 2.78 (dd, -13.6 Hz, 10.7 Hz, 1H, CHC***H***$_2$Ph), 1.74 (m, 1H, CHC***H***$_2$CH$_2$CH$_2$), 1.51 (m, 1H, CHC***H***$_2$CH$_2$CH$_2$), 1.36 (s, 9H, C(C**H**$_3$)$_3$), 1.36 & 1.24 (m, 4H C***H***$_2$C***H***$_2$CH$_2$NCO); ^{13}C NMR (150.92 MHz, $(CD_3)_2SO$) δ 200.41, 171.94, 155.90, 155.56, 137.79, 136.95, 129.20, 128.28, 128.07, 127.70, 127.53, 126.35, 77.37, 65.30, 56.54, 56.00, 40.02, 37.21, 35.04, 29.20, 28.35, 28.25, 22.52; HRMS Calcd. for $C_{29}H_{40}N_3O_7$ $[M+H]^+$: 604.2022 Found 604.2003; IR (KBr, cm^{-1}): 3295, 2929, 1668, 1660, 1527.

(S)-3-((S)-2-(benzyloxycarbonyl)-3-phenylpropanamido)-7-(tert-butoxycarbonyl)-2-oxoheptyl 2,4,6-trimethylbenzoate (5) The BMK **4** (1.73 g, 2.86 mmol) was dissolved in anhydrous DMF (20 mL) at RT under argon. Anhydrous potassium fluoride (499 mg, 8.58 mmol) and 2,4,6-trimethylbenzoic acid (517 mg, 3.15 mmol) were then added and the reaction was left to stir for 3 days at RT. Afterwards the solution was made up to 50 mL with water and extracted with dichloromethane (3 x 25 mL). The organic layer was washed with water (5 x 30 mL), saturated sodium bicarbonate (3 x 30 mL), and brine (3 x 30 mL) and then dried over magnesium sulfate. Removal of the solvent by rotary evaporation revealed a golden solid, which was recrystalized from ethyl acetate/hexanes giving a white powder. Yield (1.30 g, 67%). TLC (1:1 EtOAc:Hex): R_f =0.58; ^{1}H NMR (600.13 MHz, $(CD_3)_2SO$) δ 8.49 (d, J = 6.8 Hz, 1H, N***H***CHCOCH$_2$), 7.63 (d, J = 7.3 Hz, 1H N***H***CHCONH), 7.30 (m, 10H, ArH), 6.92 (s, 2H, Me_3C_6***H***$_2$CO), 6.75 (m, 1H CH_2N***H***CO), 5.10 (m, 2H, COC***H***$_2$O), 4.32 (m, 1H NC***H***CO in Phe and 1H NC***H***CO in Lys), 3.02 (m, 1H, CHC***H***$_2$Ph), 2.90 (m, 2H CONHC**H**$_2$), 2.82 (m, 1H, CHC***H***$_2$Ph), 2.27 (s, 6H (o-C***H***$_3$)$_3$C$_6$H$_2$CO), 2.25 (s, 3H (p-C***H***$_3$)$_3$C$_6$H$_2$CO) 1.79 (m, 1H, CHC***H***$_2$CH$_2$CH$_2$), 1.55 (m, 1H, CHC***H***$_2$CH$_2$CH$_2$), 1.36 (s, 9H, C(C**H**$_3$)$_3$), 1.36 & 1.25 (m, 4H C***H***$_2$C***H***$_2$CH$_2$NCO); ^{13}C NMR (150.92 MHz, $(CD_3)_2SO$) δ 202.92, 171.97, 168.26, 155.95, 155.54, 139.11, 137.70, 136.95, 134.94, 129.98, 129.26, 128.26, 128.085, 127.70, 127.55, 126.34, 77.31, 66.70, 65.30, 56.24, 55.92, 39.94, 37.42, 29.16, 29.03, 28.24, 22.26, 20.66, 19.29; HRMS Calcd. for $C_{39}H_{50}N_3O_7$ $[M+H]^+$: 688.3598. Found 688.3622. IR (KBr, cm^{-1}): 3314, 2929, 1711, 1661, 1522.

(S)-5-((S)-2-(benzyloxycarbonyl)-3-phenylpropanamido)-6-oxo-7-(2,4,6-

trimethylbenzoyloxy)heptan-1-aminium (6) The protected AOMK **5** (201.5 mg, 0.293 mmol) was dissolved in dichloromethane (5.3 mL) and TFA (4 mL) was added dropwise at 0°C. The solution was left to stir for 2.5 hrs, after which the solvent was concentrated by rotary evaporation. The residue was added to cold ether, and the resultant precipitate was separated via centrifuge. After decanting the liquid the white solid was dissolved in dichloromethane and coevaporated with toluene. Yield (195.9 mg, 95.3%). TLC (1:4 MeOH:DCM): R_f =0.66; ^{1}H NMR (500.13 MHz, $(CD_3)_2SO$) δ 8.53 (m, 1H, N***H***CHCOCH$_2$), 7.74 (broad s, 3H, $CH_2CH_2N\boldsymbol{H}_3$), 7.64 (m, 1H, N***H***CHCONH), 7.22 (m, 10H, ArH), 6.92 (s, 2H, $Me_3C_6\boldsymbol{H}_2CO$), 5.10 (s, 2H, PhC***H***$_2$O), 4.88 (m, 2H, COC***H***$_2$O), 4.35 (m, 1H NC***H***CO in Phe and 1H NC***H***CO in Lys), 3.03 (m, 1H, CHC***H***$_2$Ph), 2.85 (m, 2H CONHC**H**$_2$), 2.76 (m, 1H, CHC***H***$_2$Ph), 2.25 (s, 6H (o-C***H***$_3$)$_3$C$_6$H$_2$CO), 2.23 (s, 3H (p-C***H***$_3$)$_3$C$_6$H$_2$CO) 1.58 (m, 1H, CHC***H***$_2$CH$_2$CH$_2$), 1.54 (m, 1H, CHC***H***$_2$CH$_2$CH$_2$), 1.25 (m, 4H C***H***$_2$C***H***$_2$CH$_2$NH$_3$); ^{13}C NMR (125.77 MHz, $(CD_3)_2SO$) δ 202.50, 171.98, 168.21, 155.84, 139.10, 137.70, 136.90, 134.90, 129.89, 129.21, 128.21, 128.06, 127.68, 127.47, 126.32, 66.67, 65.29, 56.27, 55.62, 40.03, 37.18, 28.77, 26.47, 21.81, 20.62, 19.28; HRMS Calcd. for $C_{34}H_{42}N_3O_7$ $[M]^+$: 588.3068. Found 588.3074.

(S)-3-((S)-2-(benzyloxycarbonyl)-3-phenylpropanamido)-7-(tert-butoxycarbonyl)-2-oxoheptyl 2,6-dimethylbenzoate (7) The BMK **4** (0.1753 g, 0.29 mmol) was dissolved in anhydrous DMF (10 mL) at RT under argon. Anhydrous potassium fluoride (50.5 mg, 0.87 mmol) and 2,6-trimethylbenzoic acid (547.9 mg, 0.319 mmol) were then added and the reaction was left to stir for 3 days at RT. Afterwards the solution was made up to 25 mL with water and extracted with dichloromethane (3 x 15 mL). The organic layer was

washed with water (5 x 15 mL), saturated sodium bicarbonate (3 x 15 mL), and brine (3 x 15 mL) and dried over magnesium sulfate. Removal of the solvent by rotary evaporation revealed a golden solid, which was recrystalized from ethyl acetate/hexanes giving a white powder. Yield (0.1447 g, 74%). TLC (2:1 EtOAc:Hex): R_f =0.54; ^{1}H NMR (600.13 MHz, $(CD_3)_2SO$) δ 8.51 (d, J = 7.4 Hz, 1H, N***H***CHCOCH$_2$), 7.65 (d, J = 8.3 Hz, 1H N***H***CHCONH), 7.30 (m, 10H, ArH, and s, 1H, Me_2C_6***H***$_3$CO), 7.1 (s, 2H, Me_2C_6***H***$_3$CO), 6.76 (m, 1H CH$_2$N***H***CO), 4.9 (m, 2H, COC***H***$_2$O), 4.32 (m, 1H NC***H***CO in Phe and 1H NC***H***CO in Lys), 3.02 (m, 1H, CHC***H***$_2$Ph), 2.90 (m, 2H CONHC**H**$_2$), 2.81 (m, 1H, CHC***H***$_2$Ph), 2.3 (s, 6H (o-C***H***$_3$)$_3$C$_6$H$_2$CO), 1.79 (m, 1H, CHC***H***$_2$CH$_2$CH$_2$), 1.55 (m, 1H, CHC***H***$_2$CH$_2$CH$_2$), 1.36 (s, 9H, C(C**H**$_3$)$_3$), 1.36 & 1.25 (m, 4H C***H***$_2$C***H***$_2$CH$_2$NCO); ^{13}C NMR (150.92 MHz, $(CD_3)_2SO$) δ 207.82, 177.21, 173.35, 161.09, 160.77, 143.02, 142.19, 139.94, 138.10, 134.82, 133.50, 132.94, 131.58, 103.94, 71.89, 70.53, 61.28, 61.16, 45.17, 44.34, 42.47, 34.37, 34.29, 27.56.

(S)-5-((S)-2-(benzyloxycarbonyl)-3-phenylpropanamido)-6-oxo-7-(2,6-dimethylbenzoyloxy)heptan-1-aminium (8) The protected AOMK-II **7** (88.9 mg, 0.132 mmol) was dissolved in dichloromethane (9 mL) and TFA (3 mL) was added dropwise at 0°C. The solution was left to stir for 2.5 hrs, after which the solvent was concentrated by rotary evaporation. The residue was added to cold ether, and the resultant precipitate was separated via centrifuge. After decanting the liquid the white solid was dissolved in dichloromethane and coevaporated with toluene. Yield (195.9 mg, 93%). TLC (1:4 MeOH:DCM): R_f =0.66; ^{1}H NMR (600.13 MHz, $(CD_3)_2SO$) δ 8.56 (d, J = 7.4 Hz, 1H, N***H***CHCOCH$_2$), 7.76 (broad s, 3H, CH$_2$CH$_2$N***H***$_3$), 7.68 (m, 1H, N***H***CHCONH), 7.29 (m,

10H, ArH), 7.1 (s, 3H, $Me_3C_6\boldsymbol{H}_3CO$), 4.97 (s, 2H, $PhC\boldsymbol{H}_2O$), 4.88 (m, 2H, $COC\boldsymbol{H}_2O$), 4.38 (m, 1H $NC\boldsymbol{H}CO$ in Phe and 1H $NC\boldsymbol{H}CO$ in Lys), 3.05 (m, 1H, $CHC\boldsymbol{H}_2Ph$), 2.85 (m, 2H $CONHC\mathbf{H}_2$), 2.77 (m, 1H, $CHC\boldsymbol{H}_2Ph$), 2.30 (s, 6H $(o\text{-}C\boldsymbol{H}_3)_3C_6H_2CO$), 1.58 (m, 1H, $CHC\boldsymbol{H}_2CH_2CH_2$), 1.54 (m, 1H, $CHC\boldsymbol{H}_2CH_2CH_2$), 1.25 (m, 4H $C\boldsymbol{H}_2C\boldsymbol{H}_2CH_2NH_3$); ^{13}C NMR (150..92 MHz, $(CD_3)_2SO$) δ 202.54, 172.05, 168.16, 155.89, 137.75, 136.93, 134.70, 132.82, 129.62, 129.26, 128.30, 128.12, 127.74, 127.54, 126.38, 66.66, 65.31, 56.12, 55.63, 39.97, 37.19, 28.79, 26.51, 21.83, 19.26.

Z-Phe-Lys(Cy5)-$CH_2OCOPhMe_2$, AOMK-II(Cy5) (9) Cy5 succinimidyl ester (4 mg, 5.05 μmol) and the AOMK-II TFA salt **7** (3.1 mg, 4.59 μmol) were mixed in DMSO (600 μL) in the presence of disopropyl ethylamine (DIPEA) (2.4 μL, 13.8 μmol) for 3 hr. Water was added and the solvents were removed by lyophilization. The product was obtained by C18 reverse phase semi-preparative HPLC (method A). Yield (1.1 mg, 24%). HPLC (Method A) t_r = 8.9 min; LC-MS Calcd. for $C_{66}H_{78}N_5O_{13}S_{22}^-$ $[M]^-$: 1212.5049. Found 1212.

4-Fluoro-benzoic acid 2,5-dioxo-pyrrolidin-1-yl ester (10) 4-fluorobenzoic acid (280 mg, 2 mmol), EDC (1.917g, 10 mmol), and N-hydroxysuccinimide (1.1509 g, 10 mmol) were dissolved in DMF (10 mL) and stirred at RT under Ar. After 3.5 hr water (15 mL) was added and the precipitate extracted with diethyl ether. The organic layer was washed with water (4 x 25 mL) and brine (2 x 25 mL) and then evaporated to dryness revealing a white powder. Yield (437.8 mg, 92%).

(S)-3-((S)-2-(benzyloxycarbonyl)-3-phenylpropanamido)-7-(4-fluorobenzamido)-2-oxoheptyl 2,4,6-trimethylbenzoate (11) 4-Fluorobenzoic NHS ester (**10**) (0.237 g, 1

mmol) and the AOMK TFA salt **6** (71.9 mg, 0.1 mmol) were mixed in 5% (v/v) triethylamine in DMF (5.25 mL) for 3.5 hrs. The solution was made up to 25 mL with water and extracted with dichloromethane (3 x 25 mL). The organic layer was washed with water (3 x 25 mL), and brine (3 x 30 mL), dried over magnesium sulfate and the solvent removed by rotary evaporation. The resultant residue was purified by flash chromatography using a 1:1 (v/v) mixture of ethyl acetate/hexanes as the eluent. Yield (32.1 mg, 45%). TLC (2:1 EtOAc:Hex): R_f =0.55; ^{1}H NMR (500.13 MHz, $(CD_3)_2SO$) δ 8.53 (m, 1H, N***H***CHCOCH$_2$), 8.45 (m, 1H, CH$_2$N***H***CO), 7.89 (m, 2H in FC$_6$***H***$_4$CO), 7.64 (m, 1H, N***H***CHCONH) 7.27 (m 10H, ArH and 2H in FC$_6$***H***$_4$CO), 6.91 (s, 2H, Me$_3$C$_6$***H***$_2$CO), 5.10 (m, 2H, COC***H***$_2$O), 4.95 (s, 2H, PhC***H***$_2$O), 4.33 (m, 1H NC***H***CO in Phe and 1H NC***H***CO in Lys), 3.24 (m, 2H CONHC**H**$_2$), 2.83 (m, 1H, CHC***H***$_2$Ph), 2.80 (m, 1H, CHC***H***$_2$Ph), 2.26 (s, 6H (o-C***H***$_3$)$_3$C$_6$H$_2$CO), 2.25 (s, 3H (p-C***H***$_3$)$_3$C$_6$H$_2$CO) 1.54 (m, 1H, CHC***H***$_2$CH$_2$CH$_2$), 1.51 (m, 1H, CHC***H***$_2$CH$_2$CH$_2$), 1.23 (m, 4H C***H***$_2$C***H***$_2$CH$_2$NH$_3$); ^{13}C NMR (125.77 MHz, $(CD_3)_2SO$) δ 202.7, 172.2, 168.3, 165.1, 139.1, 137.8, 135.0, 129.8, 129.7, 129.3, 129.2, 128.3, 128.1, 127.7, 127.5, 126.4, 115.2, 115.0, 66.7, 65.3, 56.3, 55.9, 40.0, 37.4, 29.2, 22.5, 22.4, 19.4; HRMS Calcd. for $C_{41}H_{44}N_3O_7F$ $[M+H]^+$: 710.3003. Found 710.2971.

3 Development and Optimization of a Colorimetric Cathepsin B Plate Assay

3.1 Endpoint Assay

The initial approach was to develop an endpoint assay that could be applied to testing cathepsin B inhibitors. To this end, an endpoint assay was developed and optimized using the chromogenic substrate, Z-Arg-Arg-pNA (Figure 1.9) and a commercial cathepsin B inhibitor, 1-(3-Methyl-2-[(3-propylcarbamoyl-oxiranecarbonyl)-amino]-pentanoyl)-pyrrolidine-2-carboxylic (CA-074, Figure 3.1) as a positive control.

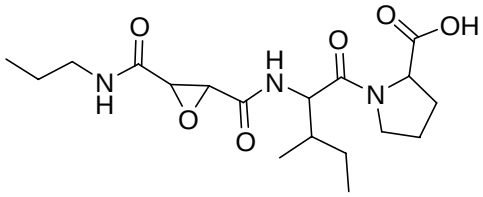

Figure 3.1 CA-074: commercial cathepsin B inhibitor

For the endpoint assay, human liver cathepsin B was added to each well of a 96 well plate with the assay buffer, containing DTT, and incubated for 15 mins at 37°C to activate the enzyme (i.e. to ensure the cysteine thiol was in its reduced form). A background absorbance was measured at 405 nm. CA-074 was added over a concentration range of 0.1 nM - 1μM and incubated for 15 mins at 37°C with the enzyme. Equal amounts of substrate was added to each well and incubated for 60 mins at 37°C after which an absorbance reading was taken again (Figure 3.2).

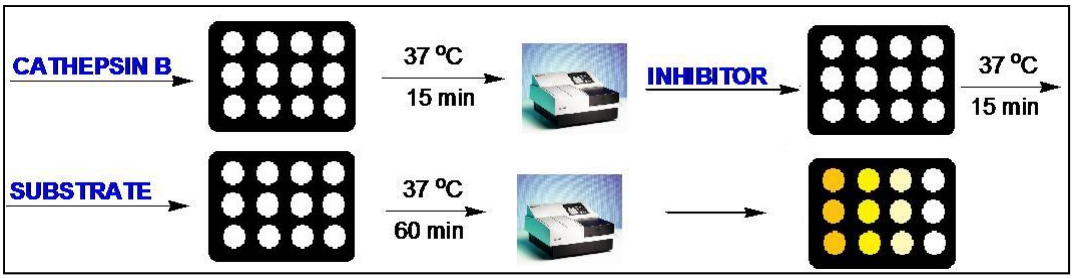

Figure 3.2 Cathepsin B endpoint assay

The experiment was repeated with different substrate concentrations (100 µM, 300 µM, and 500 µM) and 300 µM was used for further testing because it gave a measurable signal. The net absorbance was plotted against the logarithm of inhibitor concentration giving the inhibition curves which followed the typical sigmodal shape (Figure 3.3). The known inhibitor gave and IC_{50} value of 6 nM. The parent AOMK (**6**) was tested in a similar manner and an IC_{50} value of 127 nM was obtained. The experiments with **6** were repeated on the same day using the same conditions and the average IC_{50} value obtained was 126 ± 3 nM.

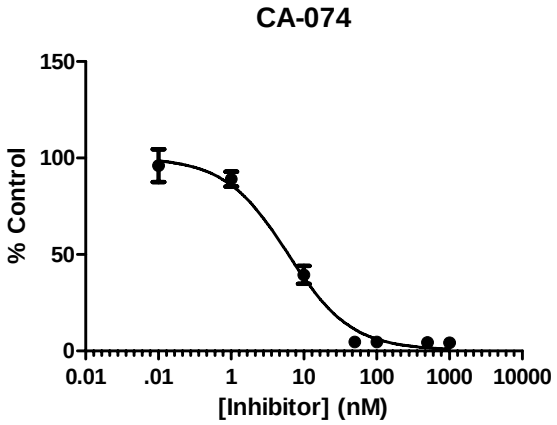

Figure 3.3 Cathepsin B inhibition with CA-074 IC_{50} = 6 nM

The IC_{50} values for competitive inhibitors (inhibitors that bind to the free enzyme at its active site) can be converted to K_i values using the Cheng-Prusoff equation:

$$Ki = \frac{IC50}{1 + \frac{[S]}{Km}}$$

where K_i is the inhibitory binding constant, IC_{50} is the concentration of inhibitor giving 50% of the maximum enzymatic response, [S] is the concentration of the substrate, and K_m is the concentration of substrate at which the initial rate is 50% of the maximum, or the Michaelis-Menten constant.[41] A K_m value of 0.9 mM was used for these calculations based on previously reported data for human liver cathepsin B.[34b] The IC_{50} values obtained for CA-074 and **6** were converted to K_i values of 5 nM and 96 nM respectively. The reported K_i values for these compounds are 4.2 nM and 170 ± 50 nM respectively.[27, 42] The CA-074 inhibitor corresponded well with the literature however the discrepancy in the value for **6** was suspicious and was later the basis for further investigation of the assay format.

AOMK II-Cy5 (**9**), and AOMK-FBz (**11**) were tested using the same procedure described above. The IC_{50} value obtained for AOMK II-Cy5 (**9**) was 9 nM (corresponding to a K_i of 7 nM) and AOMK-FBz (**11**) showed and IC_{50} of 6.4 μM. The Cheng-Prusoff equation shows the K_i is independent of substrate concentration and that at any given substrate concentration the K_i can be calculated from the IC_{50} value obtained in the experiment. The inhibitors were tested at a substrate concentration of 100 μM to confirm the K_i values. Unfortunately the K_i values obtained were different at each

substrate concentration indicating that these compounds did not fit this steady-state model.

Table 3.1 Comparision of Ki values at different substrate concentrations

Compound	K_i at [S] = 300 µM	K_i at [S] = 100 µM
CA-074	5 nM	19 nM
AOMK (6)	96 nM	32 nM
AOMK II-Cy5 (9)	7 nM	14 nM
AOMK-FBz (11)	4800 nM	not determined

3.1.1 Limitations of Endpoint Assay

Typically enzyme inhibitors function in a reversible fashion but one must consider the mode of inhibition when an enzyme reaction is studied.[43] The compounds described here are irreversible inhibitors therefore they exhibit a time-dependant inhibition of the protease.[27,44] The initial reaction is reversible then the complex undergoes a time dependent inactivation where the enzyme fully inactivated.[35c]

$$E + I \rightleftharpoons EI \longrightarrow EI^*$$

Binding constants for irreversible inhibitors don't fit the model described above because the dissociation constant K_i is dependent on enzyme concentration, preincubation time of the inhibitor with the enzyme, and substrate concentration. The typical K_i for reversible inhibitors would be independent of these factors.[45] For time-dependent inhibition the progress curves displaying product formation vs time are non-linear whereas for time-independent inhibition they are linear.[43] The more appropriate way to

characterize inhibitors that behave in this manner is to analyze these progress curves using non-linear regression with the appropriate mathematical model.[43, 45]

3.1.2 Time-dependent Inhibition

The time-dependence of inactivation was exemplified for AOMK **6**. The effect of incubation times for the inhibitor with the enzyme on activity was determined (Table 3.2). After 15 min of incubating the inhibitor with the enzyme the maximum reduction in activity was achieved. These results indicated that the reduction in the cathepsin B activity was affected by the incubation time with the inhibitor and so an alternative method to what was described in 3.1 is needed for testing the AOMK derived inhibitors.

Table 3.2 Time dependence of cathepsin B activity by **6**

	Incubation Times				
	0 min	15 min	30 min	45 min	60 min
% activity with AOMK **6**	98	60	59	58	61

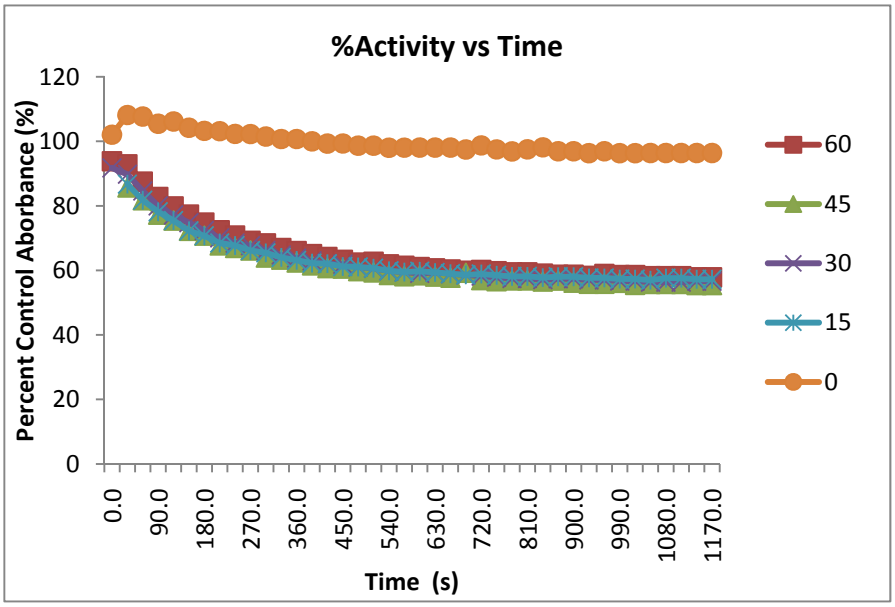

Figure 3.4 Time dependence of cathepsin B activity by **6** with preincubation times indicated at the right

3.2 Continuous Assay Development

It has been suggested that the AOMKs can be further described as suicide inhibitors.[27] A suicide inhibitor is one that produces a highly reactive species (generally electrophilic) during the enzymatic reaction, that reacts with the enzyme.[45] The suicide inhibitor inactivates in a two step mechanism resulting in the formation of a covalent bond with the enzyme. To characterize a suicide inhibitor, the kinetics of the inactivation need to be measured. This is best achieved by using a continuous enzyme assay. Because the K_i for irreversible inhibitors is related to the enzyme and substrate concentration it is important to establish an adequate enzyme concentration and an adequate substrate concentration (in relation to a determined K_m).

3.2.1 Optimization of Enzyme Concentration

When examining enzyme activity it is the initial rate at which the enzyme catalyzes the reaction under investigation that is determined. This is governed by the Michaelis-Menten equation:

$$\nu(0) = \frac{\mathrm{Vmax[S]}}{\mathrm{Km} + \mathrm{[S]}}$$

where ν_0 is the initial rate of product formation, V_{max} is the maximum rate reached, [S] is the concentration of the substrate, and K_m is the concentration of substrate at which the initial rate is 50% of the maximum, or the Michaelis-Menten constant.[46] As the concentration of the substrate increases so does the initial rate, asymptotically approaching a maximum V_{max}.[46] The initial rate of the product formation is determined from the slope of the initial linear portion of the reaction progress curve (Figure 3.5). It is important to test this in a given assay to ensure that there are sufficient data points to obtain this linear region.

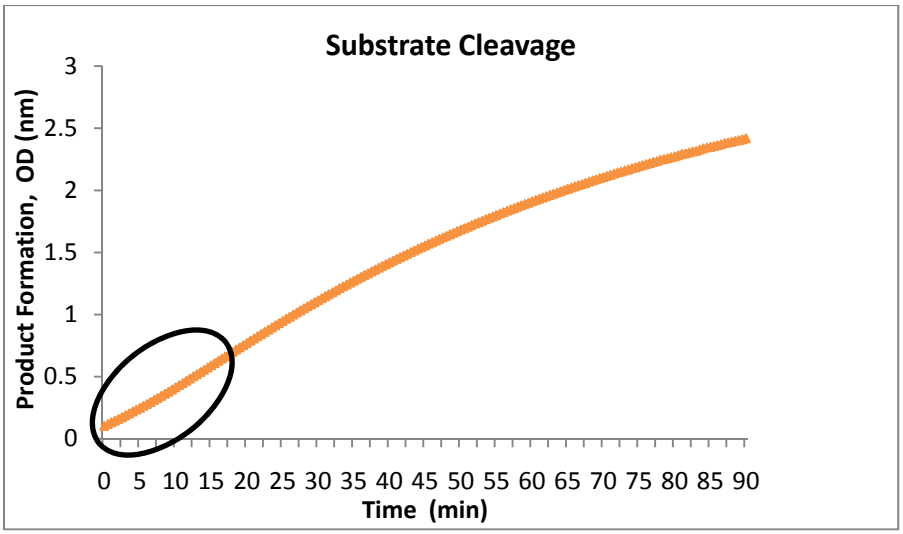

Figure 3.5 Reaction progress curve for Z-Arg-Arg-pNA cleavage (linear portion circled)

The rate of an enzymatic reaction is also dependant on the concentration of the enzyme used in the reaction. It is not surprising that as the concentration of the enzyme is increased the rate of product formation is also increased. As the concentration of the enzyme is increased, the linear portion of the reaction curve is much shorter and calculating an accurate v_0 based on the slope is difficult.[46] Therefore an optimal enzyme concentration needs to be determined to ensure accuracy in assay development. This was achieved by examining the hydrolysis of the colorimetric substrate Z-Arg-Arg-pNA by commercially available recombinant human liver cathepsin B.

A concentration range of cathepsin B ranging from 1.25 – 25 nM and a substrate concentration of 1 mM was used to determine the effect on the initial rate. The progress of the hydrolysis reaction was monitored for 73 min by measuring the absorbance or optical density (OD) at 405 nm using a plate reader (Figure 3.6).

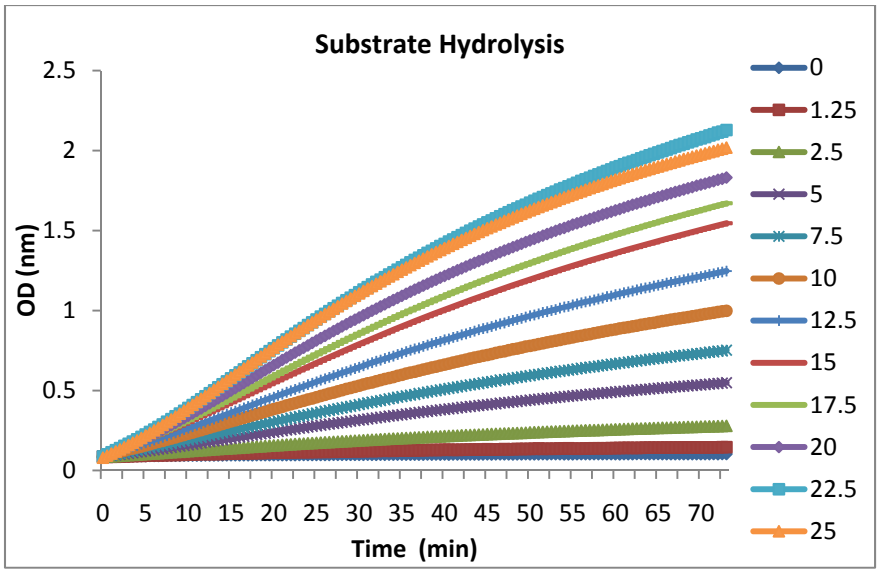

Figure 3.6 Time course of enzyme reaction with enzyme concentrations indicated at the right

The linear region was determined by calculated R-squared values for the initial time points. Data points in the first 10 min. gave R-squared values that were near 0.99 while data points over the full series gave R-squared values ranging from 0.96 – 0.99 (Table 3.3).

Table 3.3 R-square values for progress curves

Enzyme Concentration	R-square after 73 min	R-square after 10 min
1.25	0.963	0.977
2.5	0.983	0.999
5	0.990	0.999
7.5	0.991	0.999
10	0.992	0.999
12.5	0.993	0.999
15	0.992	0.998
17.5	0.990	0.998
20	0.988	0.998
22.5	0.987	0.997
25	0.980	0.997

The slopes of the progress curves were used to determine the initial rate in the first 10 min and plotted against the enzyme concentration to ensure linearity (Figure 3.7). When removing the point corresponding to [E] = 25 nM the R-squared value improved from 0.9937 to 0.9991. The enzyme concentration that was chosen was 5 nM because at this concentration the amount of product formation did not appear to reach a plateau (Figure 3.6).

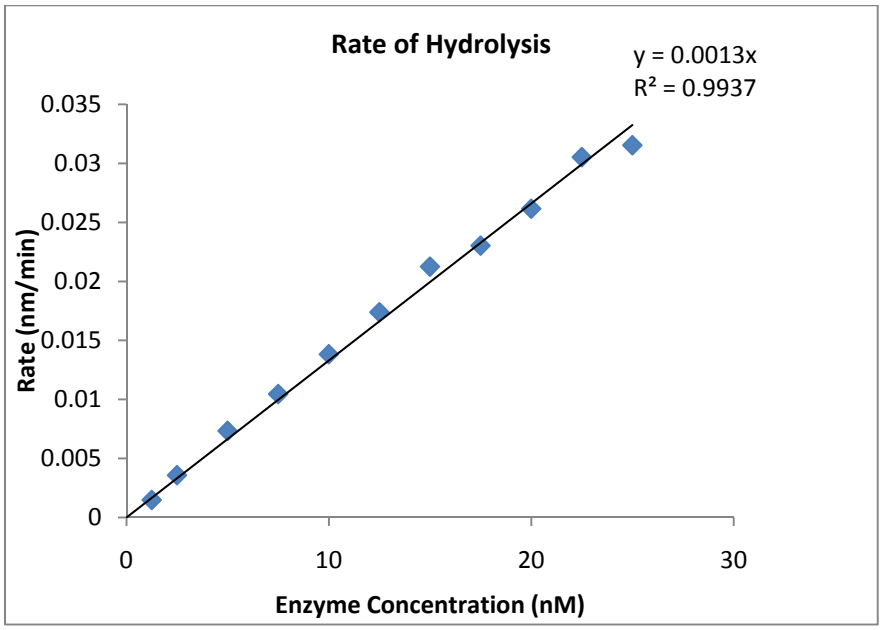

Figure 3.7 Rate of hydrolysis versus enzyme concentration

3.2.2 Determination of K_m

To determine the K_m for the cathepsin B substrate, Z-Arg-Arg-pNA, concentrations varying from 125 µM – 3mM of the substrate were used following a method by Moin *et al.*[34b] The progress of the hydrolysis reaction was monitored for 10 min by measuring the OD at 405 nm (Figure 3.8). The reaction did not appear to reach a plateau during this period.

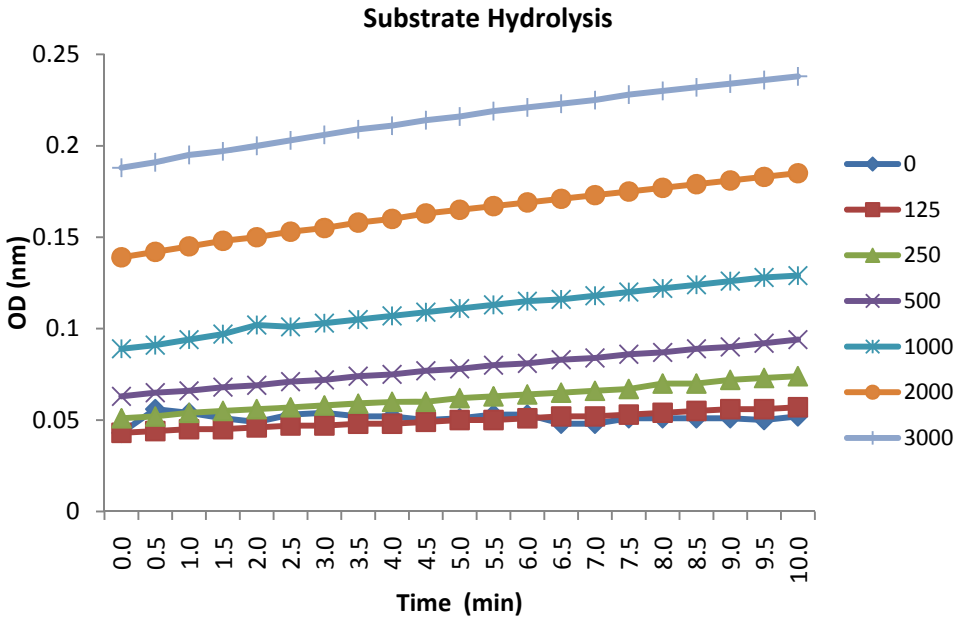

Figure 3.8 Time course of enzyme reaction at substrate concentrations in nM indicated at the right

By plotting the reaction rate versus the substrate concentration the K_m was determined using non-linear regression through the GraphPad Prism ® software (Figure 3.9). The experiment was performed in triplicate and the average K_m obtained was 390 ± 30 µM. The reported K_m values of this substrate for cathepsin B purified from human liver is reported as 900 ± 60 µM.[34b]

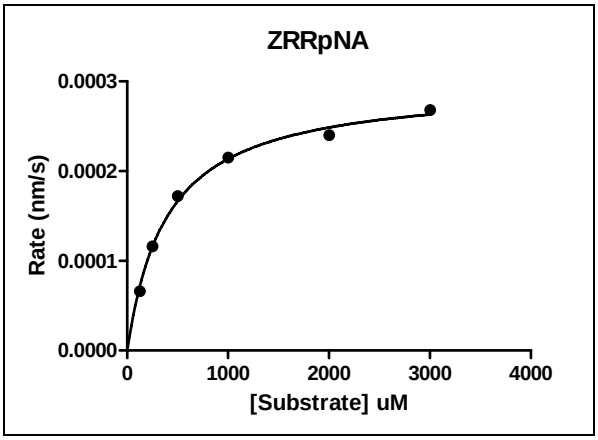

Figure 3.9 Rate of hydrolysis versus substrate concentration

The discrepancy in these values is likely due to the source of the enzyme. In a similar study performed by Hasnain *et al.*, cathepsin B was purified from rat liver and the K_m obtained was 1.01 ± 0.12 mM.[35a] The authors also tested the glycosylated recombinant rat cathepsin B and the K_m was determined to be 440 ± 30 μM, 480 ± 30 μM, and 530 ± 30 μM when obtained from 3 different pooled fractions. These values are more comparable with the values obtained in the present study. The K_m value for the cathepsin B purified from human liver is slightly lower than the K_m for cathepsin B purified from rat liver and a similar trend was observed comparing the glycosylated variants. The results can be explained by the reports that glycosylated forms of cathepsin B are less active than non-glycosylated variants.[35a, 47] Using this K_m value to calculate the K_i values for CA-074, **6**, **9**, and **11** did not eliminate the inconsistencies observed with the original assay (Table 3.4).

Table 3.4 Comparison of K_i values at different substrate concentrations using K_m = 390 nM

Compound	K_i at [S] = 300 µM	K_i at [S] = 100 µM
CA-074	3 nM	17 nM
AOMK (6)	72 nM	28 nM
AOMK II-Cy5 (9)	7 nM	12 nM
AOMK-FBz (11)	3600 nM	not determined

3.2.3 Effect of Inhibitor

Once the activity of the enzyme towards the substrate was determined, the effect of the inhibitors can be measured. To determine binding affinities for this type of inhibitor the data can be fit to an exponential equation:

$$Y = Ae^{-(kobs)t} + B$$

where Y represents the amount of product formed, k_{obs} is the rate of inhibition and A and B are constants.[45] Using non-linear regression k_{obs} values for various concentrations of inhibitor can be determined. Plots of k_{obs} vs inhibitor concentration [I] that give a straight line would indicate that saturation kinetics are not observed and the relationship is defined as:

$$kobs = \left(\frac{ki}{Ki}\right)[I]$$

where k_{obs} is the rate of inhibition, k_i is the apparent inactivation rate, and K_i is the inhibition constant. In cases where saturation is observed the relationship follows a hyperbolic fit defined as:[27, 45]

$$kobs = \frac{ki[I]}{Ki + [I]}$$

When the relationship is hyperbolic the parameters k_i and K_i can be determined independently by non-linear regression. In the case of a linear fit these parameters cannot be derived independently so alternately the second order rate constant defined as k_i/K_i is often reported following linear regression.[27] The AOMK inhibitors designed by Krantz *et al.* exhibited both linear and non-linear relationships and so it is expected that the derivatives described here could fit either of these models.

3.3 Summary and Conclusions

The original colorimetric assay that was developed can be applied to inhibitors that govern typical steady-state conditions when inhibiting cathepsin B. The AOMK inhibitors described here are time-dependant irreversible suicide inhibitors and therefore do not fit this model, therefore an alternate method is needed to assess their affinity. A continuous assay would be best suited to test these compounds. Key parameters such as the relationship between the enzyme concentration and the product formation as well as a K_m value were determined and can be applied to the development of a continuous colorimetric assay analogous to the fluorogenic assay used by Krantz *et al.*[27] The next steps would be use test the AOMK in a similar manner against the recombinant form of cathepsin B and fit it to a model where the inhibition constant or second order rate constant could be determined giving an idea of enzyme inactivation.

3.4 Experimental Section

3.4.1 Materials and Instrumentation

Human liver cathepsin B was purchased from Calbiochem. The substrate Z-Arg-Arg-pNA was from Enzo Life Sciences. Reagents used in the assay buffer were from Sigma-Aldrich. Black, clear bottom 96-well plates used were from BD Falcon. Absorbance readings were performed using a BioRad EL 808 plate reader.

3.4.2 Assay Procedures

Endpoint Assay Cathepsin B was added to a 96 well plate and preincubated for 15 min at 37°C in the assay buffer, containing 25 mM 2-(*N*-morpholino)ethanesulfonic acid (MES), 5 mM DL-Dithiothreitol (DTT), 2.5 mM disodium ethylenediaminetetraacetic acid (EDTA), and 0.001% (v/v) Tween-20 to give a final enzyme concentration of 25 nM. Following the measurement of background absorbance at 405 nm using a plate reader, CA-074 or an AOMK inhibitor was added giving final concentrations of 0.1 nM - 1μM or 1 nM – 10 μM respectively and incubated for 15 mins at 37°C with the enzyme. Z-Arg-Arg-pNA, dissolved in water was then added giving final concentrations of either 100 μM, 300 μM, or 500 μM. Following a 60 min incubation period at 37°C a final absorbance reading was measured.

Time Dependant Inhibition Cathepsin B (500 nM) was preincubated for 30 min at 37°C in a solution of 2.5 mM DTT and 0.001% (v/v) Tween-20. Constant amounts of the cathepsin B solution were added to a 96-well plate containing the assay buffer (25 mM potassium phosphate, 1 mM EDTA, 250 mM NaCl, and 3% (v/v) DMSO) resulting in enzyme concentration of 25 nM. AOMK **6** was added at 15 min intervals and

preincubated with the enzyme giving incubation times of 15, 30, 45, and 60 min for a final [S] = 100 nM. Z-Arg-Arg-pNA, dissolved in water was then added in various amounts resulting in concentrations ranging from 125μM – 3 mM. Absorbance readings were performed immediately afterwards for 20 min every 30 s at 405 nm at 37°C.

Optimization of Enzyme Concentration Cathepsin B (500 nM) was preincubated for 30 min at RT in a solution of 5 mM DTT and 0.01% (v/v) Tween-20. Various amounts of the cathepsin B solution were added to a 96-well plate containing the assay buffer (25 mM potassium phosphate, 1 mM EDTA, 250 mM NaCl, and 3% (v/v) DMSO). Various amounts of the preincubation solution were then added resulting in enzyme concentrations ranging from 1.25 – 25 nM. Z-Arg-Arg-pNA, dissolved in water was then added giving a final concentration of 1 mM. Absorbance readings were performed immediately afterwards for 73 min every 30 s at 405 nm at 37°C.

Determination of K_m Cathepsin B (200 nM) was preincubated for 30 min at RT in a solution of 5 mM DTT and 0.01% (v/v) Tween-20. Constant amounts of the cathepsin B solution were added to a 96-well plate containing the assay buffer (25 mM potassium phosphate, 1 mM EDTA, 250 mM NaCl, and 3% (v/v) DMSO) resulting in an enzyme concentration of 5 nM. Z-Arg-Arg-pNA, dissolved in water was then added in various amounts resulting in concentrations ranging from 125 μM – 3 mM. Absorbance readings were performed immediately afterwards for 20 min every 30 s at 405 nm at 37°C.

4 Summary and Future Work

The overall objective of this research was to establish a platform that could be used to identify and validate a nuclear molecular imaging agent for visualizing cathepsin B expression *in vivo*. Such an agent could be used for the detection, staging, and monitoring of highly aggressive breast cancer tumours. The platform was established by preparing a parent compound, Z-Phe-Lys-$CH_2OCOPhMe_3$ (Figure 1.6) as a targeting vector and incorporating different prosthetic groups containing radioactive signaling molecules at the *epsilon* nitrogen through different chemical links. Two examples were prepared containing fluorescent (**9**) and the fluorinated (**11**) prosthetic groups.

In parallel, steps toward the development of a colorimetric continuous assay were underway. The synthetic platform for preparing cathepsin B PET and SPECT probes has now been established. Future work will be to use the work described here to prepare and screen a library of AOMK derivatives and complete the assay development. Promising compounds should exhibit binding constants similar or better than that of the Cy5 probe **9** which has been shown to be successful. This data would then be used to modify the lead structure to optimize uptake where the resulting compound would then be used to validate the core hypothesis which is that a small molecule cathepsin B inhibitor can be modified with prosthetic groups carrying radioisotopes and be used to detect cathepsin B activity *in vivo*.

References

1. (a) Manning, H. C.; Lander, A.; McKinley, E.; Mutic, N. J., Accelerating the Development of Novel Molecular Imaging Probes: A Role for High-Throughput Screening. *J. Nucl. Med.* **2008,** *49*, 1401–1404; (b) Mather, S., Molecular Imaging with Bioconjugates in Mouse Models of Cancer. *Bioconjugate Chem.* **2009,** *20* (4), 631-643.
2. Mankoff, D. A., Molecular imaging as a tool for translating breast cancer science. *Breast Cancer Res.* **2008,** *10* (Suppl 1), S3.
3. Meikle, S. R.; Kench, P.; Kassiou, M.; Banati, a. R. B., Small animal SPECT and its place in the matrix of molecular imaging technologies. *Phys. Med. Biol.* **2005,** *50*, R45–R61.
4. Britz-Cunningham, S. H.; Adelstein, S. J., Molecular Targeting with Radionuclides: State of the Science. *J. Nucl. Med.* **2003,** *44*, 1945 - 1961.
5. Ametamey, S. M., Molecular Imaging with PET. *Chem. Rev.* **2008,** *108* (5), 1501 - 1516.
6. (a) Liu, S., Bifunctional coupling agents for radiolabeling of biomolecules and target-specific delivery of metallic radionuclides. *Adv. Drug Deliver. Rev.* **2008,** *60*, 1347 - 1370; (b) Bartholoma, M.; Valliant, J.; Maresca, K. P.; Babichc, J.; Zubieta, J., Single amino acid chelates (SAAC): a strategy for the designing of technetium and rhenium radiopharmaceuticals. *Chem. Commun.* **2009**, 493 - 512.
7. Groch, M.; Erwin, W. D., SPECT in the Year 2000: Basic Principles. *J. Nucl. Med. Technol.* **2000,** *28* (4), 233 - 244.
8. Abram, U.; Alberto, R., Technetium and Rhenium - Coordination Chemistry and Nuclear Medical Applications. *J. Braz. Chem. Soc* **2006,** *17* (8), 1486 - 1500.
9. Ehmann, W. D.; Vance, D. E., Radiochemistry and Nuclear Methods of Analysis

John Wiley & Sons, Inc.: New York, 1991; pp 313 - 345.
10. Villanueva-Meyer, J.; Leonard, M. H. J.; Briscoe, E.; Cesani, F.; Ali, S. A.; Rhoden, S.; Hove, M.; Cowan, D., Mammoscintigraphy with Technetium-99m-Sestamibi in Suspected Breast Cancer. *J. Nucl. Med.* **1996,** *37*, 926 - 930.
11. Coover, L. R.; Caravaglia, G.; Kuhn, P., Scintimammography with Dedicated Breast Camera Detects and Localizes Occult Carcinoma. *J. Nucl. Med.* **2004,** *45*, 553 - 558.
12. (a) Papantoniou, V.; Koutsikos, J.; Sotiropoulou, M.; Mainta, E.; Lazaris, D.; Tsiouris, S.; Zerva, C., Scintimammographic Findings of Phyllodes Tumor of the Breast in a Double-phase Study with Tc-99m (V)DMSA and Tc-99m MIBI: a Case Report. *Jpn. J. Clin. Oncol.* **2004,** *34* (7), 429–431; (b) Lee, J. H.; Rosen, E. L.; Mankoff, D. A., The Role of Radiotracer Imaging in the Diagnosis and Management of Patients with Breast Cancer: Part 1—Overview, Detection, and Staging. *J. Nucl. Med.* **2009,** *50*, 569 -581.
13. Miller, P. W.; Long, N. J.; Vilar, R.; Gee, A. D., Synthesis of 11C, 18F, 15O, and 13N Radiolabels for Positron Emission Tomography. *Angew. Chem. Int. Ed.* **2008,** *47*, 8998 – 9033.
14. Dehdashti, F.; Mortimer, J. E.; Siegel, B. A.; Griffeth, L. K.; Bonasera, T. J.; Fusselman, M. J.; Detert, D. D.; Cutler, P. D.; Katzenellenbogen, J. A.; Welch, M. J.,

Positron Tomographic Assessment of Estrogen Receptors in Breast Cancer: Comparison with FDG-PET and In Vitro Receptor Assays. *J. Nucl. Med.* **1995,** *36* (10), 1766 - 1774.
15. (a) Maresca, K. P.; Hillier, S. M.; Femia, F. J.; Zimmerman, C. N.; Levadala, M. K.; Banerjee, S. R.; Hicks, J.; Sundararajan, C.; Valliant, J.; Zubieta, J.; Eckelman, W. C.; Joyal, J. L.; Babich, J. W., Comprehensive Radiolabeling, Stability, and Tissue Distribution Studies of Technetium-99m Single Amino Acid Chelates (SAAC). *Bioconjugate Chem.* **2009,** *20* (8), 1625-1633; (b) Patel, S.; Gibson, R., In vivo site-directed radiotracers: a mini-review. *Nucl. Med. Biol.* **2008,** *35*, 805–815.
16. Wester, H.-J., Nuclear Imaging Probes: from Bench to Bedside. *Clin. Cancer Res.* **2007,** *13* (12), 3470 - 3481.
17. Ruth, T. J., The uses of radiotracers in the life sciences. *Rep. Prog. Phys.* **2008,** (72), 1 - 23.
18. Eckelman, W. C.; Bonardi, M.; Volkert, W. A., True radiotracers: are we approaching theoretical specific activity with Tc-99m and I-123? *Nucl. Med. Bio.* **2008,** *35* (5), 523-527.
19. Powers, J. C.; Asgian, J. L.; Ekici, O. D.; James, K. E., Irreversible Inhibitors of Serine, Cysteine, and Threonine Proteases. *Chem. Rev.* **2002,** *102* (12), 4639 - 4750.
20. Lee, M.; Fridman, R.; Mobashery, S., Extracellular proteases as targets for treatment of cancer metastases. *Chem. Soc. Rev.* **2004,** *33*, 401 - 409.
21. Lecaille, F.; Kaleta, J.; Bromme, D., Human and Parasitic Papain-Like Cysteine Proteases: Their Role in Physiology and Pathology and Recent Developments in Inhibitor Design. *Chem. Rev.* **2002,** *102* (12), 4459-4488.
22. Sloane, B. F.; Moin, K.; Krepela, E.; Rozhin, J., Cathepsin B and its endogenous inhibitors: the role in tumor malignancy. *Cancer and Metast. Rev.* **1990,** *9*, 333--352.
23. Casini, A.; Gabbiani, C.; Sorrentino, F.; Rigobello, M. P.; Bindoli, A.; Geldbach, T. J.; Marrone, A.; Re, N.; Hartinger, C. G.; Dyson, P. J.; Messori, L., Emerging Protein Targets for Anticancer Metallodrugs: Inhibition of Thioredoxin Reductase and Cathepsin B by Antitumor Ruthenium(II)-Arene Compounds. *J. Med. Chem.* **2008,** *51*, 6773–6781.
24. Illy, C.; Quraishi, O.; Wang, J.; Purisima, E.; Vernet, T.; Mort, J. S., Role of the Occluding Loop in Cathepsin B Activity. *J. Biol. Chem.* **1997,** *272* (2), 1197 - 1202.
25. Schenker, P.; Alfarano, P.; Kolb, P.; Caflisch, A.; Baici, A., A double-headed cathepsin B inhibitor devoid of warhead. *Protein Sci.* **2008,** *17*, 2145 - 2155.
26. Winnard Jr., P. T.; Pathak, A. P.; Dhara, S.; Cho, S. Y.; Raman, V.; Pomper, M. G., Molecular Imaging of Metastatic Potential. *J. Nucl. Med.* **2008,** *49* (6), 96S - 112S.
27. Krantz, A.; Copp, L. J.; Coles, P. J.; Smith, R. A.; Heard, S. B., Peptidyl (Acyloxy)methyl Ketones and the Quiescent Affinity Label Concept: The Departing Group as a Variable Structural Element in the Design of Inactivators of Cysteine Proteinases. *Biochemistry* **1991,** *30* (19), 4678 - 4687.
28. Wagner, B. M.; Smith, R. A.; Coles, P. J.; Copp, L. J.; Ernest, M. J.; Krantz, A., In vivo Inhibition of Cathepsin B by Peptidyl (Acyloxy)methyl Ketones. *J. Med. Chem.* **1994,** *37* (12), 1833 - 1840.
29. Blum, G.; von Degenfeld, G.; Merchant, M. J.; Blau, H. M.; Bogyo, M., Noninvasive optical imaging of cysteine protease activity using fluorescently quenched activity-based probes. *Nat Chem Biol* **2007,** *3* (10), 668-677.

30. Bogyo, M. S.; Blum, G.; Berger, A.; Cheng, Z.; Gambhir, S. S. Probes for In Vivo Targeting of Active Cysteine Proteases. US 20090252677A1, 2009/10/08, 2009.
31. Shokeen, M.; Anderson, C. J., Molecular Imaging of Cancer with Copper-64 Radiopharmaceuticals and Positron Emission Tomography (PET). *Accounts. Chem. Res.* **2009,** *42* (7), 832-841.
32. Maurer, T.; Fung, H. L., Comparison of methods for analyzing kinetic data from mechanism-based enzyme inactivation: application to nitric oxide synthase. *AAPS pharmSci* **2000,** *2* (1), E8.
33. Eckelman, W. C.; Kilbourn, M. R.; Mathis, C. A., Discussion of targeting proteins in vivo: in vitro guidelines. *Nucl. Med. Biol.* **2006,** *33*, 449 - 451.
34. (a) Falgueyret, J.-P.; Black, W. C.; Cromlish, W.; Desmarais, S.; Lamontagne, S.; Mellon, C.; Riendeau, D.; Rodan, S.; Tawa, P.; Wesolowski, G.; Bass, K. E.; Venkatraman, S.; Percival, M. D., An activity-based probe for the determination of cysteine cathepsin protease activities in whole cells. *Anal. Biochemistry* **2004,** *335* (2), 218-227; (b) Moin, K.; Day, N. A.; Sameni, M.; Hasnain, S.; Hirama, T.; Sloane, B. F., Human tumour cathepsin B. Comparison with normal liver cathepsin B. *Biochem. J.* **1992** *285*, 427–434; (c) Motlekar, N.; Diamond, S. L.; Napper, A. D., Evaluation of an Orthogonal Pooling Strategy for Rapid High-Throughput Screening of Proteases. *Assay Drug Dev. Techn.* **2008,** *6* (3), 395-405; (d) Turk, B.; Dolenc, I.; Zerovnik, E.; Turk, D.; Gubensek, F.; Turk, V., Human Cathepsin B Is a Metastable Enzyme Stabilized by Specific Ionic Interactions Associated with the Active Site. *Biochemistry* **1994,** *33* (49), 14800-14806.
35. (a) Hasnain, S.; Hirama, T.; Huber, C. P.; Mason, P.; Mort, J. S., Characterization of cathepsin B specificity by site-directed mutagenesis. Importance of Glu245 in the S2-P2 specificity for arginine and its role in transition state stabilization. *J of Biol. Chem* **1993,** *268* (1), 235-240; (b) Hasnain, S.; Hirama, T.; Tam, A.; Mort, J. S., Characterization of Recombinant Rat Cathepsin B and Nonglycosylated Mutants Expressed in Yeast. *J. Biol. Chem.* **1992,** *267* (7), 4713-4721; (c) Mosi, R.; Baird, I. R.; Cox, J.; Anastassov, V.; Cameron, B.; Skerlj, R. T.; Fricker, S. P., Rhenium Inhibitors of Cathepsin B (ReO(SYS)X (Where Y = S, py; X = Cl, Br, SPhOMe-p)): Synthesis and Mechanism of Inhibition. *J. Med. Chem.* **2006,** *49* (17), 5262-5272.
36. Spezzacatena, C.; Pepe, A.; Green, L. M.; Sandberg, L. B.; Bochicchio, B.; Tamburro, A. M., Synthesis, Solution Structure and Biological Activity of Val-Val-Pro-Gln, a Bioactive Elastin Peptide. *Eur. J. Org. Chem.* **2005**, 1644–1651.
37. Katritzky, A. R.; Suzuki, K.; Singh, S. K., Highly Diastereoselective Peptide Chain Extensions of Unprotected Amino Acids with N-(Z-a-Aminoacyl)benzotriazoles. *Synthesis* **2004,** (16), 2645 - 2652.
38. Blum, G.; Mullins, S. R.; Keren, K.; Fonovic, M.; Jedeszko, C.; Rice, M. J.; Sloane, B. F.; Bogyo, M., Dynamic imaging of protease activity with fluorescently quenched activity-based probes. *Nat Chem Biol* **2005,** *1* (4), 203 - 209.
39. Ngan, F.; Toofan, M., Modification of preparation of diazomethane for methyl esterification of environmental samples analysis by gas chromatography. *J. of Chromatogr. Sci.* **1991,** *29* (1), 8 - 10.

40. Guenther, K. J.; Yoganathan, S.; Garofalo, R.; Kawabata, T.; Strack, T.; Labiris, R.; Dolovich, M.; Chiraka, R.; Valliant, J. F., Synthesis and in Vitro Evaluation of 18F- and 19F-Labeled Insulin: A New Radiotracer for PET-based Molecular Imaging Studies. *J. Med. Chem* **2006,** *49*, 1466-1474.
41. (a) Yang, Y.; Hong, H.; Zhang, Y.; Cai, W., Molecular Imaging of Proteases in Cancer. *Cancer Growth and Metastasis* **2009,** *2009* (2), 13 - 27; (b) Burlingham, B. T.; Widlanski, T. S., An Intuitive Look at the Relationship of Ki and IC50: A More General Use for the Dixon Plot. *Journal of Chemical Education* **2003,** *80* (2), 214-null.
42. Mizuochi, T.; Yee, S.-T.; Kasai, M.; Kakiuchi, T.; Muno, D.; Kominami, E., Both cathepsin B and cathepsin D are necessary for processing of ovalbumin as well as for degradation of class II MHC invariant chain. *Immunology Letters* **1994,** *43* (3), 189-192.
43. Bisswanger, H., *Enzyme Kinetics Principles and Methods*. 2nd ed.; Wiley-VCH: Weinheim, 2008; p 301.
44. Montaser, M.; Lalmanach, G.; Mach, L., CA-074, But Not Its Methyl Ester CA-074Me, Is a Selective Inhibitor of Cathepsin B within Living Cells. *Biological Chemistry* **2002,** *383*, 1305 - 1308.
45. Marangoni, A. G., *Enzyme Kinetics : A Modern Approach*. Wiley: Hoboken, 2003; p 247.
46. Jambovane, S.; Duin, E. C.; Kim, S.-K.; Hong, J. W., Determination of Kinetic Parameters, Km and kcat, with a Single Experiment on a Chip. *Anal. Chem.* **2009,** *81* (9), 3239-3245.
47. Mach, L.; Stuwe, K.; Hagen, A.; Ballaun, C.; Gossl, J., Proteolytic processing and glycosylation of cathepsin B The role of the primary structure of the latent precursor and of the carbohydrate moiety for cell-type-specific molecular forms of the enzyme. *Biochem. J.* **1992,** (282), 577-582.